Feasibility of intranasal delivery of thin-film freeze-dried, mucoadhesive AS01$_B$-adjuvanted vaccine powders

Yu-Sheng Yu[1,5], Khaled AboulFotouh[1], Gerallt Williams[2], Julie Suman[2], Chris Cano[3], Zachary N. Warnken[4], Robert O. Williams III[1], Zhengrong Cui[1*]

1. The University of Texas at Austin, College of Pharmacy, Division of Molecular Pharmaceutics and Drug Delivery, Austin, Texas, USA
2. Aptar Pharma, Le Vaudreuil, France
3. TFF Pharmaceuticals, Inc. Fort Worth, TX, USA
4. Via Therapeutics, Inc. Austin, Texas, USA
5. National Taiwan University, Department of Chemical Engineering, Taipei, Taiwan

* Correspondence should be sent to: Zhengrong.cui@austin.utexas.edu

Abstract

Intranasal vaccination by directly applying a vaccine dry powder is appealing. However, a method that can be used to transform a vaccine from a liquid to a dry powder and a device that can be used to administer the powder to the desired region(s) of the nasal cavity are critical for a successful intranasal vaccination. In the present study, using a model vaccine that contains the liposomal $AS01_B$ as an adjuvant and ovalbumin (OVA) as a model antigen, it was shown that thin-film freeze-drying can be applied to convert the liquid vaccine containing sucrose at a sucrose to lipid ratio of 15:1 (w/w), in the presence or absence of carboxymethyl cellulose sodium salt (CMC) as a mucoadhesive agent, into dry powders. Ultimately, the thin-film freeze-dried $AS01_B$/OVA vaccine powder containing 1.9% w/w of CMC (i.e., TFF $AS01_B$/OVA/$CMC_{1.9\%}$ powder) was selected for additional evaluation because the TFF $AS01_B$/OVA/$CMC_{1.9\%}$ powder was mucoadhesive and maintained the integrity of the antigen and the physical properties of the vaccine. Compared to the TFF $AS01_B$/OVA powder that did not contain CMC, the TFF $AS01_B$/OVA/$CMC_{1.9\%}$ powder had a lower moisture content and a higher glass transition temperature and was more porous. In addition, the TFF $AS01_B$/OVA/$CMC_{1.9\%}$ thin films were relatively thicker than the TFF $AS01_B$/OVA thin films without CMC. When sprayed with the Unit Dose System Powder (UDSP) nasal device, the TFF $AS01_B$/OVA powder and the TFF $AS01_B$/OVA/$CMC_{1.9\%}$ powder generated similar particle size distribution curves, spray patterns, and plume geometries. Importantly, after the TFF $AS01_B$/OVA/$CMC_{1.9\%}$ powder was sprayed with the UDSP nasal device, the integrity of the OVA antigen and the $AS01_B$ liposomal adjuvant did not change. Finally, a Taguchi L8 orthogonal array was applied to identify the optimal parameters for using the UDSP device to deliver the TFF $AS01_B$/OVA/$CMC_{1.9\%}$ vaccine powder to the middle and lower turbinate and the nasopharynx regions in both adult and

child nasal casts. Results from this study showed that it is feasible to apply the TFF technology to transform a nasal vaccine candidate from liquid to a dry powder and then use the UDSP nasal device to deliver the TFF vaccine powder to the desired regions in the nasal cavity for intranasal vaccination.

Keywords: Vaccine, powder, freeze-drying, pediatric vs. adult, deposition, intranasal

1. Introduction

Intranasal vaccination is an attractive, non-invasive route of vaccine administration. Intranasal vaccine can induce specific immune responses not only systemically, but also in the mucosal secretions of the respiratory tract (Birkhoff et al., 2009), which is advantageous as many pathogens infect their hosts through the respiratory tract (Chavda et al., 2021). In fact, several nasal vaccines have been approved for human use around the world, including the FluMist Quadrivalent in the United States (US) (Suryadevara and Domachowske, 2014), Fluenz Tetra in the European Union (EU) (Gasparini et al., 2021), NASOVAC-S in India (Ortiz et al., 2015), a freeze-dried nasal live influenza vaccine (Ganwu®) by the Changchun BCHT Biotechnology in China, and recently a nasal Coronavirus disease 2019 (COVID-19) vaccine by Bharat Biotech in India. Those nasal vaccines are live (attenuated) influenza virus-based or adenovirus-based and are presented as a liquid suspension or a freeze-dried powder for reconstitution. The liquid vaccine suspension is then administered intranasally using a nasal sprayer. Intranasal administration of vaccine directly as a dry powder has advantages, including ease of storage and distribution (Flood et al., 2016), extended residence time in the nasal cavity, and a higher dose of vaccine that can be administered. Unfortunately, vaccine dry powders with the proper aerosol properties for deposition in the desired region(s) in the nasal cavity and a method to prepare the dry powders remain needed.

Thin-film freeze-drying is a bottom-up dry powder engineering technology. It involves the ultra-rapid thin-film freezing (TFF) of a liquid (e.g., solution, suspension, or emulsion) on a cryogenically cooled solid surface (Engstrom et al., 2008; Overhoff et al., 2009). The liquid is dropped as droplets (e.g., 2 mm in diameter) from about 1 cm to 10 cm above the

cryogenically cooled solid surface. Upon impact onto the cooled surface, the droplet rapidly spreads into a thin film, which is then frozen into a thin film. Solvent such as water in the frozen thin films is removed by lyophilization. Dry powder engineering using the TFF technology is advantageous over other similar dry powder engineering technologies such as conventional shelf freeze-drying, spray drying, and spray freeze-drying in that it avoids or minimizes shear stress and heat stress, while generating powders that are generally highly porous, brittle (Hufnagel et al., 2022), and having large specific surface area (Wang et al., 2021), making them potentially feasible for directly intranasal administration. Conversely, the TFF process is associated with a relative larger liquid-solid interface between the liquid droplets and the cryogenically cooled solid surface. Previously, it has been shown that the TFF technology can be applied to produce dry powders of various vaccines, including vaccines adjuvanted with aluminum salts (Alzhrani et al., 2021; Li et al., 2015; Thakkar et al., 2018), (nano)emulsions such as MF59 or AddaVax (AboulFotouh et al., 2022a), and liposomes such as AS01$_B$ (AboulFotouh et al., 2022b).

Herein, a model vaccine comprised of ovalbumin (OVA) as a model antigen and the liposomal AS01$_B$ as an adjuvant was used to test the feasibility of using the TFF technology to prepare dry powder vaccines for direct intranasal administration. All currently approved human nasal vaccines are virus-based and do not contain any adjuvant. The AS01$_B$ was chosen in this study because a recent report from our group showed that AS01$_B$-containing vaccines can be converted to dry powders by TFF (AboulFotouh et al., 2022b). Results from a recent study have demonstrated the safety and efficacy of AS01$_B$ as a potential nasal vaccine adjuvant in a mouse model (Sato-Kaneko et al., 2022). Moreover, one can find in the literature intranasal immunization studies wherein the vaccines contain either

121 monophosphoryl lipid A (MPL) or QS21 as the adjuvant (Baldridge et al., 2000; Sasaki et
122 al., 1998a; Sasaki et al., 1998b), and the liposomal AS01$_B$ contains both MPL and QS21.
123
124 To increase the residence time of the vaccine in the nasal cavity, various mucoadhesive
125 agents have been included in the vaccine formulation, and their effect on the vaccine was
126 studied. The mucoadhesive agents studied include chitosan, sodium alginate, gelatin, and
127 sodium carboxymethylcellulose (CMC), each with its own unique mechanism(s) of
128 interaction with the mucosa (Dekina et al., 2016; Grabovac et al., 2005; Kesavan et al.,
129 2010; Sogias et al., 2008). A challenge is that the mucoadhesive agent can interact with the
130 AS01$_B$/OVA vaccine and change the structure of the AS01$_B$, the antigen, and/or the vaccine.
131 Therefore, the effect of the mucoadhesive agents on the AS01$_B$/OVA vaccine before and
132 after being subjected to thin-film freeze-drying with sucrose as an excipient was studied.
133 One of the mucoadhesive agents at a concentration that showed no detectable effect on the
134 physical properties of the AS01$_B$/OVA vaccine was chosen for further characterization.
135 Aptar's unit dose system powder (UDSP) nasal device was used to characterize the particle
136 size distribution, spray pattern, and plume geometry of selected AS01$_B$/OVA vaccine
137 powders upon actuation. Finally, the deposition patterns of a selected AS01$_B$/OVA vaccine
138 powder following actuation using the UDSP nasal device into 3D printed nasal casts based
139 on the CT-scan images of the noses of an adult and a child were evaluated to predict the
140 feasibility of using the UDSP nasal device to deliver thin-film freeze-dried vaccine
141 powders (TFF vaccine powders) directly into the posterior nasal cavity and the
142 nasopharynx regions of human nasal cavity (Warnken et al., 2018). Unlike in infants, in
143 children older than two years and in adults, the Waldeyer's ring in the naso-oropharynx
144 region is the key lymphoid tissue in the nasal cavity (Davis, 2001; Debertin et al., 2003).

Therefore, for an intranasal vaccine to induce specific immune responses, the vaccine needs to be delivered either directly to the nasopharynx region or to the posterior nasal cavity and then move by means of ciliary clearance to the naso-oropharynx region following the mucous blanket posterior movement. Within the posterior nasal cavity, delivery of the vaccine to the upper turbinate region, where the olfactory bulb resides, should be avoided or minimized to reduce the access of the vaccine to the brain via the olfactory nerves (Cai et al., 2022; Xu et al., 2021b).

2. Materials and Methods

2.1. Materials

Albumin from chicken egg white (ovalbumin, OVA), chitosan medium molecular weight, sodium alginate, gelatin, CMC, MPL from *Salmonella enterica* serotype minnesota Re 595 (Re mutant), porcine mucin type III, and 2-mercaptoethanol were from Sigma-Aldrich (St. Louis, MO). QS-21 was from Dessert King International (San Diego, CA). Sucrose was from Millipore (Billerica, MA). Anhydrous ethanol (EtOH) was from Decon Labs (King of Prussia, PA). Cholesterol was from MP Biomedicals (Santa Ana, CA). The 1,2-dioleoyl-sn-glycero-3-phosphocholine (DOPC) was from Avanti Polar Lipids, Inc. (Alabaster, AL). Fluorescein isothiocyanate isomer I (FITC) was from Acros Organics (Geel, Belgium). Dulbecco's phosphate-buffered saline (DPBS, pH 7.0-7.3, 9.5 mM) was from Gibco (Grand Island, NY). Laemmli sample buffer 4× and Coomassie G-250 were from Bio-Rad (Hercules, CA). Blue prestained protein standard was from New England Biolabs (Ipswich, MA). Artificial nasal mucus was from Biochemazone (Leduc, Alberta, Canada). HYDRANAL™ - Coulomat AG was from Honeywell (Charlotte, NC). The UDSP nasal device was kindly donated by AptarGroup, Inc. (Crystal Lake, IL). All chemicals were used as received without further purification.

2.2. Preparation of the AS01$_B$/OVA model vaccine

To prepare the AS01$_B$/OVA model vaccine, the liposomal adjuvant was prepared first as described before (AboulFotouh et al., 2022b). Briefly, 4.0 mg of DOPC, 1.0 mg of cholesterol, and 0.2 mg of MPL were dissolved with 1.25 mL of EtOH in a 20 mL glass vial. A lipid membrane was formed in the vial by evaporating the ethanol under gentle

nitrogen flow. Next, 0.5 mL of DPBS was added to the vial to rehydrate the lipids, and the mixture was stirred overnight at room temperature. The final concentration of DOPC in the liposome suspension was 8 mg/mL. The liposome suspension was sonicated with a probe sonicator (Qsonica Q700) until the particle size reached about 100 nm based on dynamic light scattering (DLS). The AS01$_B$/OVA model vaccine was prepared by adding 50 μg of QS-21, 50 μg of OVA, and 19.5 mg of sucrose to 125 μL of the liposome suspension, and the final volume was adjusted to 500 μL with DPBS.

2.3. Preparation of AS01$_B$/OVA model vaccines with different mucoadhesive agents

To prepare the AS01$_B$/OVA model vaccine with different concentrations of chitosan, sodium alginate, gelatin, or CMC, 50 μg of QS-21, 50 μg of OVA, and 19.5 mg of sucrose were first added to 125 μL of liposome suspension. The stock solution of chitosan was prepared by dissolving chitosan in a 0.1 M acetic acid aqueous solution (2% w/v). The stock solutions of sodium alginate, gelatin, and CMC were prepared by dissolving them in DPBS (2% w/v). Different volumes of the solutions containing mucoadhesive agents were then added to the AS01$_B$/OVA vaccine to achieve a final concentration of 0.1%, 0.2%, 0.4%, 1%, w/v, corresponding to 1.9%, 3.7%, 7.2%, and 16.3% (w/w) of the mucoadhesive agents to the total weight of all components in the vaccine formulation except water. The final volume of the AS01$_B$/OVA vaccines was then adjusted to 500 μL with DPBS.

2.4. Thin-film freeze-drying of the AS01$_B$/OVA model vaccines

The as-prepared AS01$_B$/OVA vaccines, with or without mucoadhesive agents, were converted into dry powders by the TFF process. First, the liquid vaccines were frozen into small thin films following the reported single-vial TFF process (Xu et al., 2021a). Briefly,

a 20 mL glass vial was placed on dry ice until the temperature reached equilibrium. The liquid vaccine was added dropwise with a BD 1 mL syringe with a 21G needle to the bottom of the vial to form frozen thin films. The frozen films were then freeze-dried in a lyophilizer (SP VirTis AdVantage Pro). The lyophilization cycle was -40°C for 20 h, gradually ramping from -40°C to 25°C in 20 h, and then 25°C for 20 h. The chamber pressure was maintained at 80 mTorr. After lyophilization, the vials were backfilled with nitrogen gas, capped, crimped, and stored at room temperature.

2.5. Determination of particle size and zeta potential

A Malvern Nano ZS (Westborough, MA) was used to measure the particle size and zeta potential of the liposomes and the vaccines. The vaccine powder was reconstituted with deionized water (DI water) at a volume identical to the volume of the liquid vaccine before it was subjected to TFF. Samples were diluted 50 times with DPBS. The final pH value of all the samples was approximately 7.2 to 7.4.

2.6. Evaluation of the integrity of the OVA and the liposome

Sodium dodecyl sulfate–polyacrylamide gel electrophoresis (SDS-PAGE) was applied to evaluate the integrity of OVA in AS01$_B$/OVA vaccines before and after they were subjected to thin-film freeze-drying, as well as before and after the vaccine powders were sprayed with an Aptar UDSP nasal device. Vaccine powders were reconstituted with water. To spray a powder, the powder was filled into a UDSP nasal device following the manufacturer's instruction and sprayed into a glass pipette rubber head. The powder was then reconstituted from within the rubber head with water. For SDS-PAGE analysis, the sample was mixed with Laemmli sample buffer 4× containing 10% 2-mercaptoethanol, boiled for 10 min at

100°C, and then loaded into a well of a 4–20% precast polyacrylamide gel from Bio-Rad (Hercules, CA) (30 µL per well). The blue prestained protein standard was also loaded to the gel. The electrophoresis was performed at 90 V for 90 min. The SDS-PAGE gel was stained with Coomassie G-250, and the gel image was captured with a camera.

Scanning transmission electron microscope (STEM) was utilized to examine the integrity of the liposomes after the vaccine powder was sprayed with a UDSP nasal device. The vaccine powder was reconstituted and diluted 5 times with water and then transferred to a glow discharge-treated carbon coated copper grid from Electron Microscopy Sciences (Hatfield, PA). The sample was stained with a 2% uranyl acetate solution for 2 min and then air dried. Finally, the STEM images were captured with a Hitachi S5500 (Tokyo, Japan) available in the Texas Materials Institute at UT Austin.

2.7. In vitro mucoadhesion test

The *in vitro* mucoadhesion test was done following a previously reported procedure with modifications (Trenkel and Scherließ, 2021). To simulate the human nasal mucosal tissue, 10 cm Petri dishes were coated with two different solutions: 1.5% (w/v) agar in DPBS (pH = 6) or 1.5% (w/v) agar plus 2% (w/v) porcine mucin in DPBS (pH = 6). The coating layer was solidified by incubating the Petri dishes for 2 h at room temperature followed by 30 min at 4°C. After solidification, the coated dishes were incubated at 32°C in a Fisher Scientific incubator-shaker (Hampton, NH) until equilibrium (shaking not applied), and 3-5 mg of the vaccine films were gently placed onto the gel. The dishes were then turned vertically and incubated for 2 h at 32°C. The maximum downward movement of the vaccine powders at the time points of 10 min, 20 min, 30 min, 1 h, and 2 h were recorded.

2.8. Characterization of the TFF vaccine powders

XRD was done using a Rigaku R-Axis Spider (Tokyo, Japan) available at UT Austin. Vaccine powder was mounted in mineral oil and loaded onto the sample loops. The powder was irradiated with Cu Kα radiation, and the diffraction pattern was captured with a 2-D detector. The 2-D pattern was then converted to 1-D pattern. The crystal structures of the sodium chloride (NaCl) and sucrose were obtained from the Crystallography Open Database (COD) (http://www.crystallography.net), and the reference patterns were generated with a Cambridge Crystallographic Data Center (CCDC) Mercury software. Also, the crystallite sizes (τ) of the samples were calculated using the Scherrer equation:

$$\tau = \frac{K\,\lambda}{\beta\,\cos\theta}$$

Where K is the shape factor 0.9, λ is the Cu Kα radiation wavelength, β is the full width at half maximum (FWHM) of the peaks, and θ is the Bragg angle.

To obtain the scanning electron microscope (SEM) images of a sample, a film of the TFF AS01$_B$/OVA or the TFF AS01$_B$/OVA with 1.9% CMC was placed onto the conductive carbon tape. The sample was then sputtered with a layer of Au/Pd (60:40) (40 mA, 1 min). SEM images were taken with a Hitachi S5500 with an acceleration voltage of 20 kV.

The surface profiles of the thin films were measured with Keyence VK-X1100 profilometer (Osaka, Japan) available at UT Austin. Before the measurement, a vaccine thin film was placed onto the unpolished side of the silicon wafer with the top up. The 3D reconstructed images of the film were captured with a 2.5 × objective lens while the ring light source was utilized. The thickness of the film was calculated with the Keyence Multi File Analyzer

288 software.

289

290 The residue water content in vaccine powder was determined by Karl Fischer titration using
291 a Mettler Toledo C20 coulometer (Columbus, OH). Briefly, 2.5 mL of Coulomat AG
292 solution was drawn from the solution tank and injected into the vial containing the powder
293 with a gas-tight syringe. The solution was mixed well with the powder, and 2.0 mL of the
294 mixture was then injected back to the solution tank. The amount of water in the samples
295 was then determined by the instrument, and the water content (%) in the samples was
296 calculated with the following equation:

297

298 $$\text{Water content (\%)} = \frac{\text{Amount of water (mg)}}{\text{Solid content of the sample being injected (mg)}}$$

299

300 Temperature-modulated differential scanning calorimetry (mDSC) was performed using a
301 TA Instruments Q20 differential scanning calorimeter (New Castle, DE) available at UT
302 Austin. Briefly, 3-5 mg of the powder was loaded to the Tzero hermetic pan from TA
303 Instruments. The scanning range was from -20 to 250°C. The temperature was modulated
304 ±1.0°C every 60 s. The data were analyzed with the TA Instruments TRIOS software.

305

306 ***2.9. Plume geometry, spray pattern, and the particle size distribution of the aerosolized***
307 ***powder***

308 The spray pattern and the plume geometry of the TFF vaccine powders were captured with
309 an in-house built laser sheet system (Warnken et al., 2018). To study the plume geometry
310 of a vaccine powder, the powder was loaded into a UDSP nasal device and sprayed upward.

Images were captured with a camera at a rate of 500 frames per second. To identify the boundary of the plume, the Fiji software (https://imagej.net/software/fiji) was used to create the z-stacking images from different time points to measure the plume angle. For the spray pattern, the vaccine powder was loaded into a UDSP nasal device and sprayed upward, and the laser sheet was located 6 cm above the tip. The images were captured at an angle of 45° and a frame rate of 500 frames per second. The Fiji software was then used to create the z-stacking images, and the perspective correction of the images was performed with MATLAB R2021b software. The ovality and the area were then measured with the Fiji software.

To measure the particle size distribution of the sprayed vaccine powder, the powder was filled into a UDSP nasal device and sprayed to measure the particle size with Malvern Spraytec. During the experiment, the device was fixed with a clamp, and the angle was adjusted to 30° above to the horizontal plane. The distance between the tip and the laser spot was 6 cm, while the device to lens distance was 9 cm. The device was actuated manually, and the laser diffraction signal was recorded at a frame rate of 2500 Hz.

SEM was also utilized to examine the particles after the vaccine powder was sprayed with a UDSP nasal device. The SEM specimen mount was first covered with a non-porous carbon tape. The vaccine powder was then sprayed onto the carbon tape at a distance of 6 cm. The sample was then sputtered with Au/Pd (60:40) (40 mA, 1 min), and the images were captured with an acceleration voltage of 20 kV.

2.10. Deposition pattern of the TFF vaccine powder

For this experiment, FITC-labeled OVA (i.e., OVA-FITC) was used to prepare the AS01$_B$/OVA-FITC vaccine with 1.9% CMC. The detailed preparation procedure of the OVA-FTIC is in Supplementary Material S1.

The two 3D-printed nasal casts based on the CT-scan images of a male of 48 years of age and a female of 7 years of age were used to perform the deposition test (Warnken et al., 2018). The inner surface of the nasal cast was coated with an artificial nasal mucus, and the excess fluid was purged with air. The TFF AS01$_B$/OVA/CMC$_{1.9\%}$ vaccine powder (OVA labeled with FITC) was loaded into a UDSP nasal device and sprayed into the left nostril of the nasal cast. The coronal angle and sagittal angle were 0° or 20° and 45° or 60°, respectively. The definitions of the coronal angle and the sagittal angle are shown in **Fig. sup1**. The insertion depth was 0.5 cm for the 48-year-old male nasal cast and 0.4 cm for the 7-year-old female nasal cast. To determine the effect of breathing on the deposition pattern, the nasal cast was connected to a vacuum pump to evaluate the effect of flow rate on the deposition pattern. The flow rate was set at 0 or 10 litter per min (LPM) for the 48-year-old male nasal cast and 0 or 5 LPM for the 7-year-old nasal cast. For three parameters (i.e., coronal angle, sagittal angle, and flow rate), each with 2 levels, the Taguchi L8 orthogonal array (**Table 1**) was used to find their optimal combination.

After the powder was aerosolized, the nasal cast was disassembled into the following parts: (1) vestibule, (2) upper turbinate, (3) middle turbinate, (4) lower turbinate, (5) nasopharynx, and (6) filter. Each part was rinsed with 5 mL of water. The fluorescence intensities of the solutions were measured with a BioTek Microplate Reader (Winooski, VT). The amount of powder deposited in each part was calculated based on a calibration curve constructed

359 with FITC-labeled vaccine powder dissolved in water.

360

361 The delivery efficiency of the powder using the UDSP nasal device was calculated based
362 on the following equation:

363 $$\text{Delivery efficiency (\%)} = \frac{\text{Amount of the powder delivered (mg)}}{\text{Amount of the powder loaded in the UDSP (mg)}} \times 100\%$$

364

365 The recovery percentage of the vaccine powder in the nasal cast was defined as:

366 $$\text{Recovery percentage (\%)} = \frac{\text{Total amount of the powder recovered (mg)}}{\text{Amount of the powder delivered (mg)}}$$

367 Where the total amount of the powder recovered was based on the fluorescence intensity
368 measurement.

369

370 The deposition efficiency of the vaccine powder in a specific part or region of the nasal
371 cast was defined as:

372 $$\text{Deposition efficiency (\%)} = \frac{\text{Amount of the powder recovered in each part (mg)}}{\text{Amount of the powder recovered (mg)}} \times 100\%$$

373

374 Finally, the total amount of the powder recovered in the desirable region (i.e., middle
375 turbinate, lower turbinate, and nasopharynx region) was defined as the regional deposition
376 efficiency (RDP).

377

378 To identify the optimized conditions for the RDP, the signal to noise (S/N) ratio was
379 calculated for each parameter at different levels based on the “larger the better”
380 characteristic of the Taguchi method (Ghani et al., 2004).

$$\text{S/N ratio} = -10 \times \log\left(\frac{1}{n}\sum_{i=1}^{n}\left(\frac{1}{y_i^2}\right)\right)$$

Where n is the number of observations for each parameter, and y is the average of the observation (i.e., RPD).

Table 1. The Taguchi L8 orthogonal array for studying the deposition patterns of the TFF vaccine powder in two different nasal casts

Run #	Coronal Angle	Sagittal Angle	Flow Rate (LPM)	
			48-year-old	7-year-old
1	0°	45°	0	0
2	20°	60°	0	0
3	20°	45°	10	5
4	0°	60°	10	5

2.11 Statistical analysis

Statistical analysis was performed with Microsoft Office Excel or OriginLab OriginPro 2022b. Data are presented as mean ± standard deviation (SD), and the number of the replication (n) was indicated in the figure caption.

3. Results and Discussions

3.1. Preparation and thin-film freeze-drying of the AS01$_B$/OVA model vaccine

AS01$_B$ is a liposomal adjuvant comprised of DOPC, cholesterol, MPL, and QS21. AS01$_B$ is prepared by adding QS21 in preprepared liposomes comprised of DOPC, cholesterol, and MPL (1:0.25:0.05, w/w) (AboulFotouh et al., 2022b). The DOPC/cholesterol/MPL liposomes prepared had a hydrodynamic diameter of 101.3 ± 5.3 nm (n = 7). The AS01$_B$/OVA vaccine was then prepared by mixing the liposome suspension with a solution of OVA and a solution of QS21. Data from a previous study from our group showed that sucrose at a sucrose to lipid ratio of 15:1 (w/w) protected the AS01$_B$/OVA vaccine during thin-film freeze-drying (AboulFotouh et al., 2022b). **Fig. 1** shows the particle size distribution curves of the AS01$_B$/OVA vaccine before and after it was subjected to thin-film freeze-drying and reconstitution. As expected, there was not any significant change in the particle size distribution after the vaccine was subjected to thin-film freeze-drying.

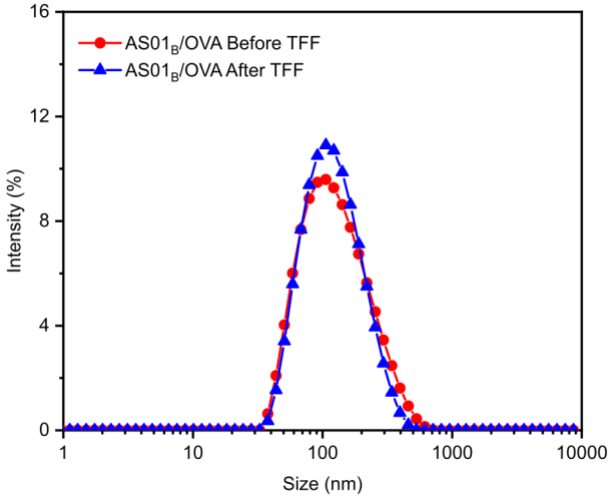

Fig. 1. Representative particle size distribution curves of the AS01$_B$/OVA vaccine before and after it was subjected to thin-film freeze-drying and reconstitution.

3.2. Identification of an AS01B/OVA vaccine formulation with a mucoadhesive agent

A mucosal adhesive agent is needed in the AS01B/OVA vaccine to increase its residence time in the nasal cavity. Chitosan, sodium alginate, gelatin, or CMC was added into the AS01B/OVA vaccine as a mucoadhesive agent to reach a final concentration of 0, 1.9%, 3.7, 7.2, or 16.3% by weight (vs. total weight of the vaccine except water), and the particle size and zeta potential values of the formulations before and after they were subjected to thin-film freeze-drying and reconstitution were determined. As shown in **Fig. sup2A**, adding sodium alginate, gelatin, and CMC at 7.2% (w/w) or below did not affect the particle size of AS01B/OVA vaccine, while chitosan at all concentrations tested caused a significant increase in the particle size, which might be due to the relatively small zeta potential value of the AS01B/OVA with chitosan (**Fig. sup2B**). After thin-film freeze-drying and reconstitution, only the AS01B/OVA vaccine formulations with gelatin or CMC at the concentrations of 1.9% or 3.7% by weight maintained their particle size (**Fig. sup2C**). Overall, adding the mucoadhesive agents changed the zeta potential value of the AS01B/OVA vaccine (**Fig. sup2B, D**), which was not surprising as all mucoadhesive agents tested were expected to have a certain extent of ionization at pH 7.2 to 7.4. However, subjecting the AS01B/OVA vaccine formulations to thin-film freeze-drying did not significantly affect their zeta potential values (**Fig. sup2B, D**). Shown in **Fig. 2A, B, C** are the particle sizes, particle size distribution curves, and zeta potential values of the AS01B/OVA vaccine formulations with CMC at 1.9%, 3.7%, 7.2%, or 16.3%, w/w, before and after they subjected to thin-film freeze-drying and reconstitution. Clearly, the particle size distribution profiles in the vaccine formulations containing 1.9% or 3.7% (w/w) of CMC were preserved after they were subjected to thin-film freeze-drying. The zeta potential values of the AS01B/OVA vaccines with CMC did not significantly change after

437 they were subjected to thin-film freeze-drying (**Fig. 2C**), although it is unclear why the
438 zeta potential value of the AS01$_B$/OVA vaccine without CMC became more negative (**Fig.**
439 **2C**). Therefore, the AS01$_B$/OVA vaccine formulations with CMC at 1.9% or 3.7% (w/w)
440 were chosen for further study.
441

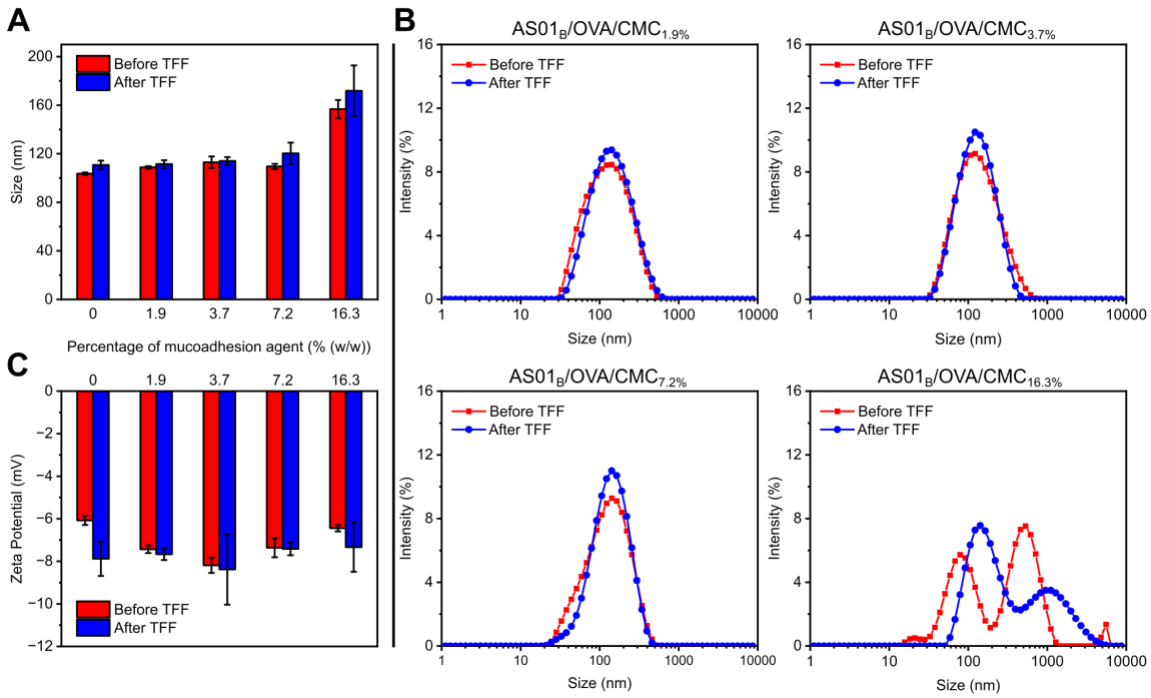

442

443 **Fig. 2.** AS01$_B$/OVA with different concentrations of CMC as a mucoadhesive agent.
444 Shown are (A) particle size, (B) representative particle size distribution curve, and (C)
445 zeta potential. Data in A and C are mean ± S.D. (n = 3).
446

447 ***3.3. The integrity of the OVA before and after the AS01$_B$/OVA vaccine formulations with***
448 ***CMC were subjected to thin-film freeze-drying***

449 To evaluate the impact of the thin-film freeze-drying process on the integrity of OVA
450 antigen, SDS-PAGE was used to analyze the AS01$_B$/OVA vaccine formulations containing
451 0, 1.9%, or 3.7% of CMC. The original OVA in solution (**Fig. 3**, lane I) showed two bands

around 43 kDa, which might be attributed to the different glycosylated forms of OVA. A close comparison of **Fig. 3** lanes II vs. III, lanes IV vs. V, and lanes VI vs. VII did not show any apparent difference, indicating that the integrity of OVA was maintained, regardless of the content of the CMC in the vaccine formulations. SDS-PAGE analysis with the individual component of the $AS01_B$/OVA vaccine formulations confirmed that the broad bands below 11 kDa shown in the $AS01_B$/OVA samples (**Fig. 3**) were from the liposomes (**Fig. sup3**).

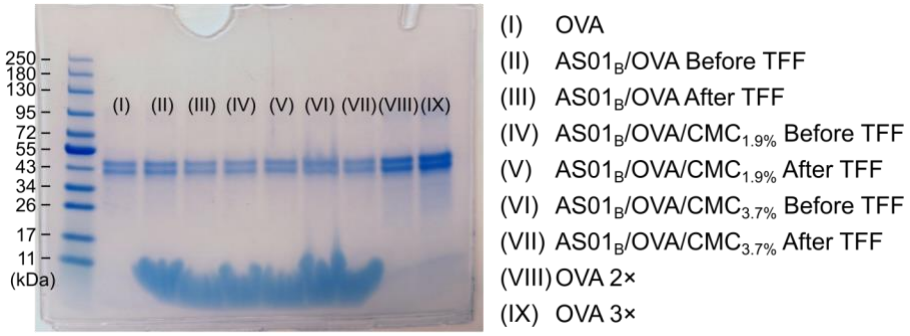

Fig. 3. SDS-PAGE image of $AS01_B$/OVA with 0, 1.9%, or 3.7% of CMC before and after they were subjected to thin-film freeze-drying and reconstitution.

3.4. In vitro mucoadhesion test

Petri dishes coated with 1.5% agar or 1.5% agar plus 2% porcine mucin were used to simulate the surface of human mucosal tissue. In the in vitro mucoadhesion test, films of TFF $AS01_B$/OVA powders with 0, 1.9%, or 3.7% of CMC were placed on the agar or agar plus porcine mucin layer. The dishes were turned vertically and incubated at 32°C (**Fig. 4A**). The thin films swelled due to the moisture in the gel or the atmosphere and flowed down slowly. The maximum traveling distances of the formulations at different time points are shown in **Fig. 4B**.

With the gel containing 1.5% agar only, the displacement of the TFF AS01$_B$/OVA powder almost reached 6 cm after 10 min of incubations, while the displacements of TFF AS01$_B$/OVA vaccine powders with 1.9% or 3.7% CMC were only 1.5 cm and 2 cm, respectively, during the same time period. The displacement of the TFF AS01$_B$/OVA vaccine powders with 1.9% and 3.7% CMC both reached ~4.5 cm after 1 h of incubation, indicating that the CMC in the AS01$_B$/OVA vaccine rendered the vaccine powders adhesive to agar gel.

With the gel containing 1.5% agar and 2% porcine mucin, the displacements of all three TFF vaccine powders decreased significantly. However, the displacement of the TFF AS01$_B$/OVA powder without CMC was still larger than that of TFF AS01$_B$/OVA powders with 1.9% or 3.7% CMC (**Fig. 4B**). The displacement of the TFF AS01$_B$/OVA powder with 1.9% CMC was slightly smaller than that with 3.7% CMC. Therefore, the TFF AS01$_B$/OVA vaccine with 1.9% CMC (AS01$_B$/OVA/CMC$_{1.9\%}$) was selected for further study.

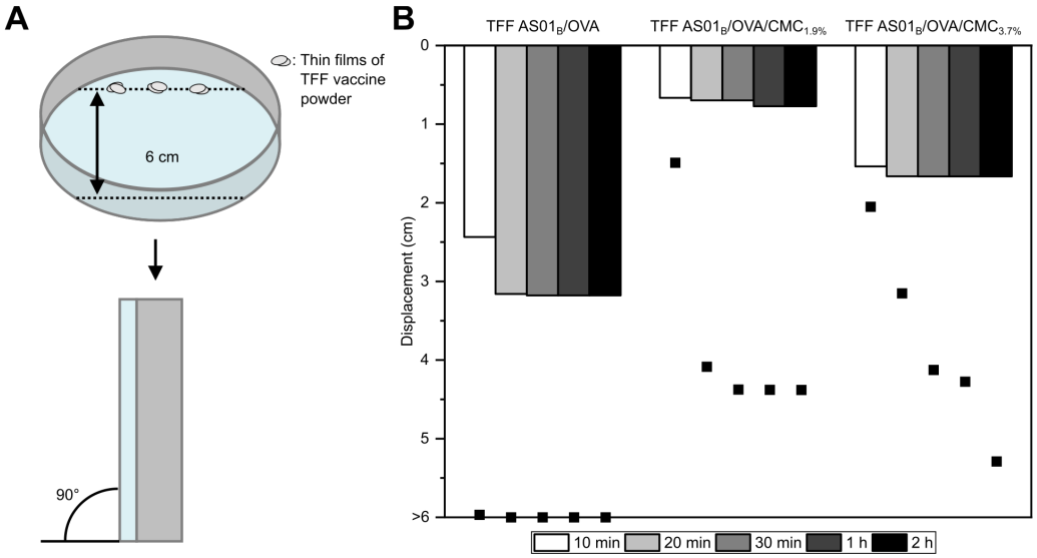

Fig. 4. In vitro mucoadhesion test. (A) Experimental design. (B) Displacement of TFF $AS01_B$/OVA vaccine powders with or without 1.9% or 3.7% CMC on 1.5% agar gel (dots) or 1.5% agar plus 2% porcine mucin gel (bars).

3.5. Characterization of the TFF $AS01_B$/OVA vaccine powders with 0 or 1.9% CMC

The residue water content in the TFF vaccine powders is important to their stability and aerosol properties. The moisture contents in the TFF $AS01_B$/OVA powder and the TFF $AS01_B$/OVA/$CMC_{1.9\%}$ powder were 3.29 ± 0.21% and 1.78 ± 0.14%, respectively. The CMC in the TFF $AS01_B$/OVA/$CMC_{1.9\%}$ sample likely made the sucrose matrix less hygroscopic.

Surface profilometer was used to characterize the surface of the TFF vaccine powders. **Fig. 5A and 5B** show the images of the thin films of TFF $AS01_B$/OVA powders with 0 or 1.9% of CMC. It appears that the TFF $AS01_B$/OVA film was more porous compared to the TFF $AS01_B$/OVA/$CMC_{1.9\%}$ film. In addition, the TFF $AS01_B$/OVA/$CMC_{1.9\%}$ film had a radial pattern, which was likely because the nucleation process of the sucrose was altered by the CMC during the TFF process. The mean thickness of the TFF films was determined using six randomly selected films of the TFF $AS01_B$/OVA vaccine powders with 0 or 1.9% CMC. The mean thickness of the TFF $AS01_B$/OVA/$CMC_{1.9\%}$ films was 228.7 ± 51.1 μm, about 37% larger than that of the TFF $AS01_B$/OVA films (i.e., 167.3 ± 44.4 μm). Considering that the distance between the needle tip and the cryogenically cooled surface was fixed, it is likely that the CMC in the $AS01_B$/OVA vaccine made the vaccine droplets difficult to completely spread upon impact on the cooled surface during the TFF process. It is also

possible that for the AS01$_B$/OVA vaccine, without CMC, the sucrose was less prone to collapse during the drying process.

The microscopic structures of the TFF vaccine powders were examined using SEM. The SEM images (**Fig. 5C-F**) (both top view and bottom view) revealed that the TFF AS01$_B$/OVA and AS01$_B$/OVA/CMC$_{1.9\%}$ films were porous. However, the TFF AS01$_B$/OVA/CMC$_{1.9\%}$ sample looked more fibrous than the TFF AS01$_B$/OVA sample (**Fig. 5C-D**), likely due to the presence of the CMC in the formulation. Moreover, minor phase separation was observed in both samples. The small particles deposited on the sucrose matrix were likely crystals of the buffer salts.

One important factor affecting the integrity of the vaccine formulation during the freezing and subsequent sublimation process was the crystallization of the excipients. XRD was used to characterize the crystalline properties of TFF powders (**Fig. 6A**). The peaks at 27.5°, 31.8°, 45.6°, 56.7°, 66.5°, and 75.6 on the patterns of TFF AS01$_B$/OVA and TFF AS01$_B$/OVA/CMC$_{1.9\%}$ powders were identified as the (111), (200), (220), (222), (400), and (420) planes of NaCl according to its simulated pattern. The crystallite sizes of the NaCl in TFF AS01$_B$/OVA and AS01$_B$/OVA/CMC$_{1.9\%}$ powders were 23.0 nm and 22.5 nm, respectively, as calculated using the Scherrer equation. Peaks unique to sucrose were not present, indicating that sucrose remained amorphous in the TFF vaccine powders, which is in agreement with previous findings with other sucrose-containing TFF powders (AboulFotouh et al., 2022b; Zhang et al., 2021), and is desirable for maintaining the integrity of the vaccine during TFF process.

534 **Fig. 6B** shows the DSC profiles of the TFF AS01$_B$/OVA and AS01$_B$/OVA/CMC$_{1.9\%}$
535 samples. Their glass transition temperatures (T_g) were 6.87°C and 32.66°C, respectively.
536 Because it was reported that freeze-dried samples would crystalize and collapse when
537 being stored at a temperature above their T_g (te Booy et al., 1992), it was concluded that
538 the TFF AS01$_B$/OVA/CMC$_{1.9\%}$ powder could provide better stability while stored at a
539 temperature equal to or below room temperatures. Of course, different sugars and polymers
540 may be included in the powders to further increase their T_g, and thus thermostability, if
541 needed. The DSC profiles of TFF AS01$_B$/OVA and AS01$_B$/OVA/CMC$_{1.9\%}$ powders both
542 showed a major endotherm peak around 189°C, which is likely due to the melting of
543 sucrose (Beckett et al., 2006). The mechanism underlying the smaller peak located left of
544 the main melting endotherm of sucrose in both TFF AS01$_B$/OVA and AS01$_B$/OVA/CMC$_{1.9\%}$
545 powders is unknown. However, considering that there were several components in the TFF
546 powders and sucrose is prone to decomposition during the melting process (Lu et al., 2017),
547 the melting endotherm of sucrose could be distorted (Bhandari and Hartel, 2002).
548

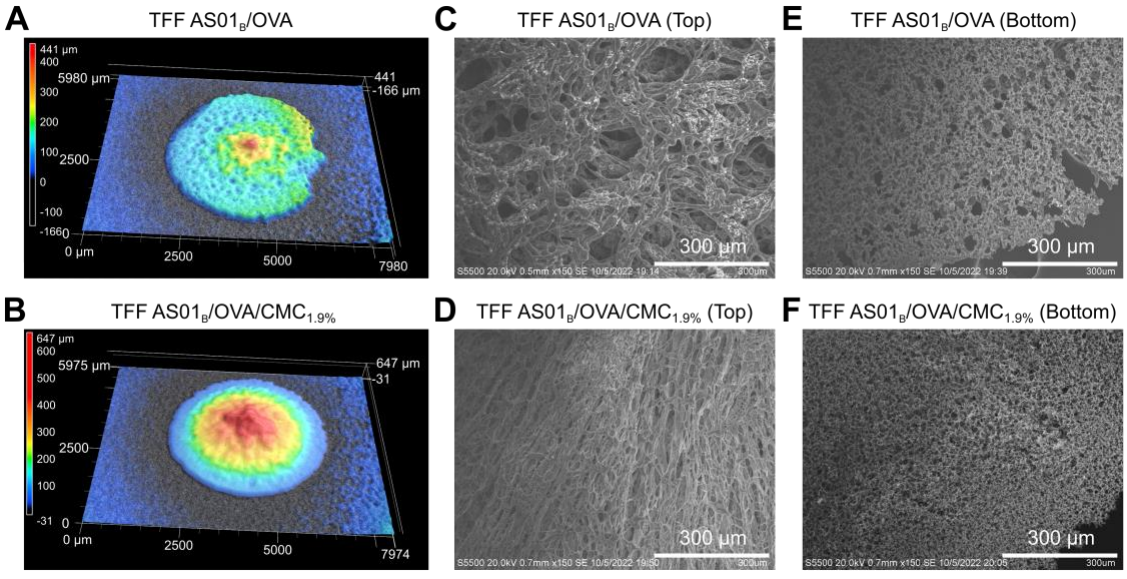

549

Fig. 5. Characterization of TFF AS01$_B$/OVA and AS01$_B$/OVA/CMC$_{1.9\%}$ films. Shown in A-B are representative surface profiles of the TFF AS01$_B$/OVA (A) and TFF AS01$_B$/OVA/CMC$_{1.9\%}$ films (B). (C-D) Representative SEM images (top view) of the TFF AS01$_B$/OVA (C) and AS01$_B$/OVA/CMC$_{1.9\%}$ films (D). (E-F) Representative SEM images (bottom view) of the TFF AS01$_B$/OVA (E) and AS01$_B$/OVA/CMC$_{1.9\%}$ films (F).

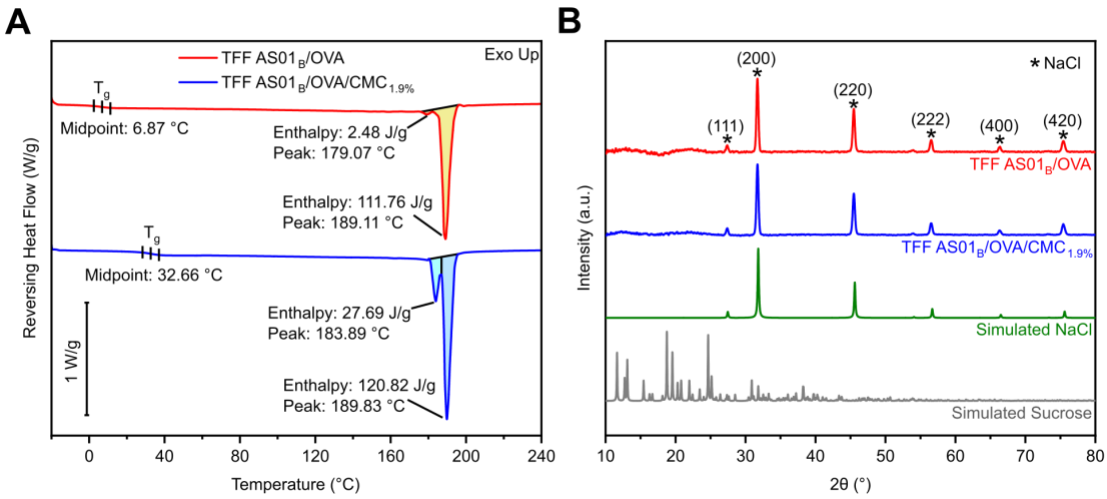

Fig. 6. (A) The XRD diffractograms of the TFF vaccine powders and the simulated patterns of NaCl (COD: 1000041) and sucrose (COD: 3500015). (B) The DSC profiles of the TFF vaccine powders.

3.6. Spraytec analysis of the thin-film freeze-dried AS01$_B$/OVA vaccine powders sprayed with a UDSP nasal device

The AS01$_B$/OVA vaccine powder was filled into the UDSP nasal device manually (~19 mg per device) and sprayed to characterize the particle size distribution using laser diffraction. The existing FDA's draft guidelines for size distribution characterization by laser diffraction only cover sprayed liquid formulations. The spray is divided into the initial

phase, the fully developed phase, and the dissipation phase. According to the transmission profile shown in **Fig. 7A**, the TFF AS01$_B$/OVA vaccine powder sprayed with the UDSP nasal device did not have an obvious fully developed (or stable) phase. Instead, the transmission reached a minimum around 3 milliseconds (ms) after the actuation and then rapidly recovered to the maximum within 14 ms; this result matched the time-course images of the sprayed powder captured by a high-speed camera (**Fig. 7B**). Therefore, the particle size at 4 ms centered around the minimum transmission was integrated, which was more representative compared to that in the recommended fully developed phase.

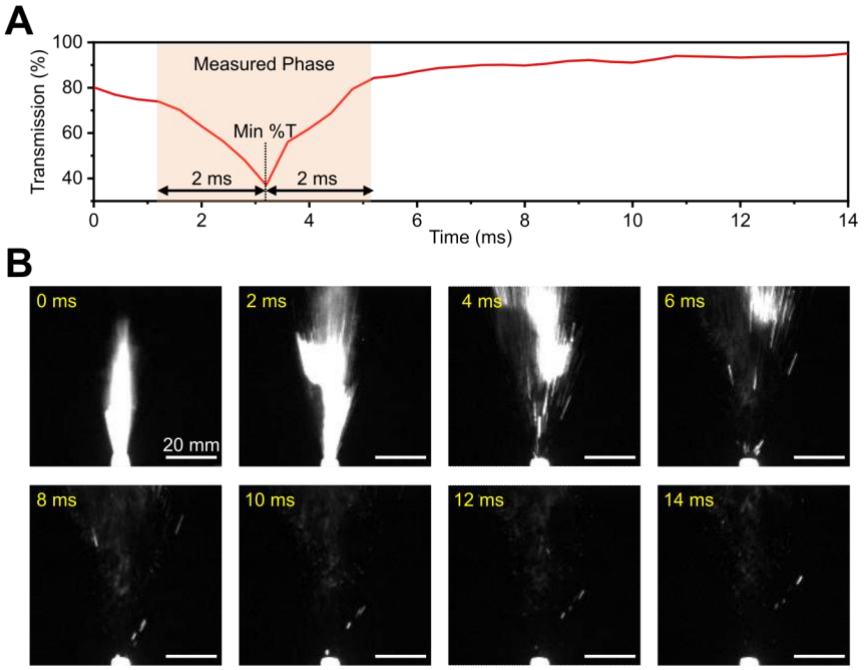

Fig. 7. (A) A representative transmission profile of the TFF AS01$_B$/OVA vaccine powder and (B) the time course images of the TFF AS01$_B$/OVA powder sprayed with the UDSP nasal device.

Figs. 8A and **B** show the particle size distribution of the TFF AS01$_B$/OVA and the TFF AS01$_B$/OVA/CMC$_{1.9\%}$ powders, which had a median particle size by volume (Dv(50))

582 value of 311.9 ± 1.3 μm and 224.2 ± 12.0 μm, respectively. The %V < 10 μm values for
583 the TFF AS01$_B$/OVA powder and the AS01$_B$/OVA/CMC$_{1.9\%}$ powder were 0.66 ± 0.09 %
584 and 0.51 ± 0.09 %, respectively (**Fig. 8A, B**).
585
586 SEM was used to examine the sprayed powders of the TFF AS01$_B$/OVA and the
587 AS01$_B$/OVA/CMC$_{1.9\%}$ vaccines (**Fig. 8C, D**). The particles of sprayed powders were not
588 uniform, showing a wide size distribution, and the particles of the sprayed TFF
589 AS01$_B$/OVA/CMC$_{1.9\%}$ powder were generally smaller than that of sprayed TFF
590 AS01$_B$/OVA powder, which agreed with the Spraytec results (**Fig. 8A, B**). Although there
591 were small particles in the background of sprayed TFF AS01$_B$/OVA powder and
592 AS01$_B$/OVA/CMC$_{1.9\%}$ powder (**Fig. 8C, D**), the contribution of those particles to the
593 volume frequency was insignificant compared to large particles, which agrees with the
594 unimodal distribution of the particle size based on the Spraytec result (**Fig. 8A, B**). Also,
595 since most of the small particles were larger than 10 μm, the risk of the particles entering
596 the lung after intranasal administration in humans is minimized, indicating that it is suitable
597 to use the UDSP nasal device for intranasal administration of the TFF vaccine powders.
598
599 ***3.7. The plume geometry and spray pattern of the thin-film freeze-dried AS01$_B$/OVA***
600 ***vaccine powders sprayed with the UDSP nasal device***
601 The plume geometry and the spray pattern of the TFF AS01B/OVA vaccine powder were
602 studied after the powder was sprayed using a UDSP nasal device and shown in **Fig 9**. The
603 plume angles of the TFF AS01$_B$/OVA powder and the TFF AS01$_B$/OVA/CMC$_{1.9\%}$ powder
604 were 24.90 ± 4.05° and 24.52 ± 4.81°, respectively. Statistical analysis of the spray pattern
605 shows that the area of the pattern was 367.70 ± 48.96 mm^2 for the TFF AS01$_B$/OVA powder

606 and 361.70 ± 55.83 mm^2 for the TFF AS01$_B$/OVA/CMC$_{1.9\%}$ powder. Both powders had
607 good ovality values, i.e., 1.28 ± 0.11 for the TFF AS01$_B$/OVA powder and 1.22 ± 0.08 for
608 the TFF AS01$_B$/OVA/CMC$_{1.9\%}$ powder. Overall, it was concluded that including the CMC
609 at 1.9% w/w in the AS01$_B$/OVA vaccine did not significantly affect the spray pattern and
610 plume geometry of the powder after spraying using the UDSP nasal device.
611

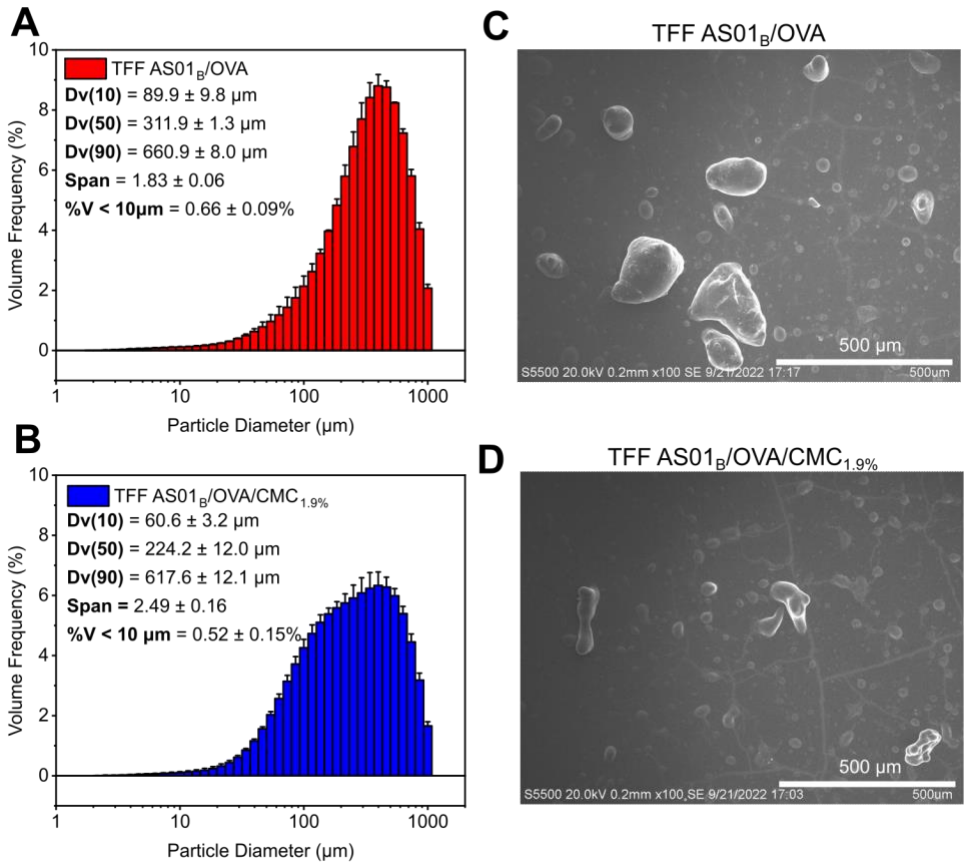

612

613 **Fig. 8.** (A-B) The particle size distribution curves of (A) TFF AS01$_B$/OVA and (B) TFF
614 AS01$_B$/OVA/CMC$_{1.9\%}$ powders sprayed using a UDSP nasal device and determined using
615 a Spraytec spray particle size analyzer. (**C-D**) Representative SEM images of TFF
616 AS01$_B$/OVA powder and TFF AS01$_B$/OVA/CMC$_{1.9\%}$ powder after they were sprayed
617 using a UDSP nasal device.

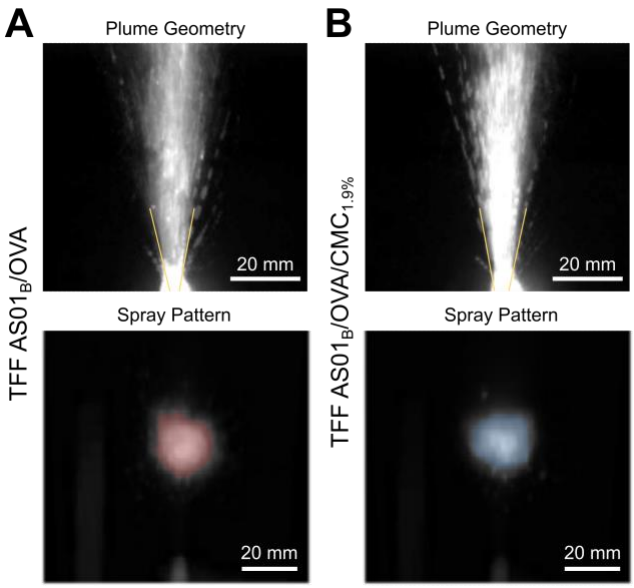

618

619 **Fig. 9.** The plume geometries and spray patterns of the TFF $AS01_B$/OVA and the TFF

620 $AS01_B$/OVA/$CMC_{1.9\%}$ powders after they were sprayed using a UDSP nasal device.

621

622 ***3.8. The integrity of the OVA and the $AS01_B$ after the $AS01_B$/OVA vaccine powders were***

623 ***sprayed using the UDSP nasal device***

624 The integrity of the OVA after the TFF $AS01_B$/OVA powder was aerosolized using the

625 UDSP nasal device was evaluated using SDS-PAGE. As shown in **Fig. 10A**, a comparison

626 of the OVA bands in lanes II vs. III and lanes IV vs. V did not reveal fragmentation or

627 aggregation of the OVA protein in the TFF $AS01_B$/OVA powder and the TFF

628 $AS01_B$/OVA/$CMC_{1.9\%}$ powder. Clearly, the OVA protein in the $AS01_B$/OVA vaccine

629 powders was not sensitive to the shear stress associated with spraying them with the UDSP

630 nasal device.

631

632 STEM was also used to characterize the TFF $AS01_B$/OVA/$CMC_{1.9\%}$ powder before and

633 after it was sprayed with the UDSP nasal device (**Fig. 10B, C**). The liposomes in the TFF

AS01$_B$/OVA/CMC$_{1.9\%}$ powder before and after being sprayed with the UDSP nasal device were about 100 nm. Also, no obvious liposome aggregation was observed after the TFF AS01$_B$/OVA/CMC$_{1.9\%}$ powder was sprayed, indicating that the liposomes in the TFF AS01$_B$/OVA/CMC$_{1.9\%}$ vaccine powders were also not sensitive to the shear stress associated with spraying them with the UDSP nasal device.

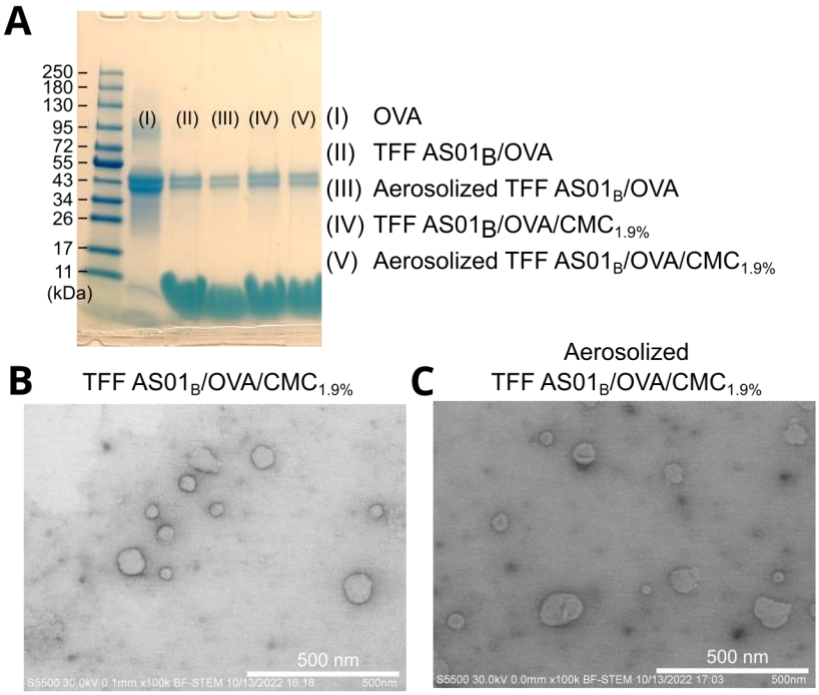

Fig. 10. The integrity of the AS01$_B$/OVA vaccine powder before and after being sprayed with the UDSP nasal device. (A) The SDS-PAGE image of the TFF AS01$_B$/OVA and the AS01$_B$/OVA/CMC$_{1.9\%}$ before and after they were sprayed. (B) Representative STEM images of TFF AS01$_B$/OVA/CMC$_{1.9\%}$ powder before and after it was sprayed using a UDSP device.

3.9. Deposition patterns of the TFF AS01$_B$/OVA/CMC$_{1.9\%}$ *vaccine powder in nasal casts*

649 The TFF $AS01_B$/OVA/$CMC_{1.9\%}$ powder was manually loaded into the UDSP nasal device
650 at 22.99 ± 1.58 mg (n = 27). After actuation, the delivered amount of the TFF
651 $AS01_B$/OVA/$CMC_{1.9\%}$ powder was 21.69 ± 1.60 mg. In other words, the delivery
652 efficiency was 94.46 ± 4.87%.
653
654 The deposition pattern of the TFF $AS01_B$/OVA/$CMC_{1.9\%}$ in the nasal cast based on the CT
655 scan of a 48-year-old male is shown in **Fig. 11A-B**. In all the conditions, the majority of
656 the TFF powder was deposited in the middle and lower turbinate and the nasopharynx
657 regions. When an air flow of 10 LPM was applied to the nasal cast, the deposition
658 percentage in the nasopharynx region and the filter increased, which is expected. The
659 percentage deposited in the upper turbinate region where the olfactory bulb resides was
660 less than 10% in all the conditions, indicating that the exposure of the vaccine powder to
661 the olfactory bulb can be minimized by spraying the TFF vaccine powder with the UDSP
662 nasal device. As shown in **Fig. 11C**, the RDP of Run #1 had the highest value of 84.4%,
663 and the Run #2 showed the lowest value of 71.3%. To evaluate the effect of each parameter
664 on the RDP, the S/N ratios were calculated. Since a higher S/N ratio will lead to a higher
665 RDP, it was concluded that the optimal condition for the RDP in the nasal cast based on a
666 48-year-old male is: 0° for the coronal angle, 45° for the sagittal angle, and 0 LPM for the
667 flow rate, which is the same as Run #1 (**Fig. 11D**). Finally, since the difference of the S/N
668 ratio between two levels indicates the impact of the parameter on the RDP, it was concluded
669 that the order of the impact on RDP was sagittal angle > coronal angle > flow rate.
670

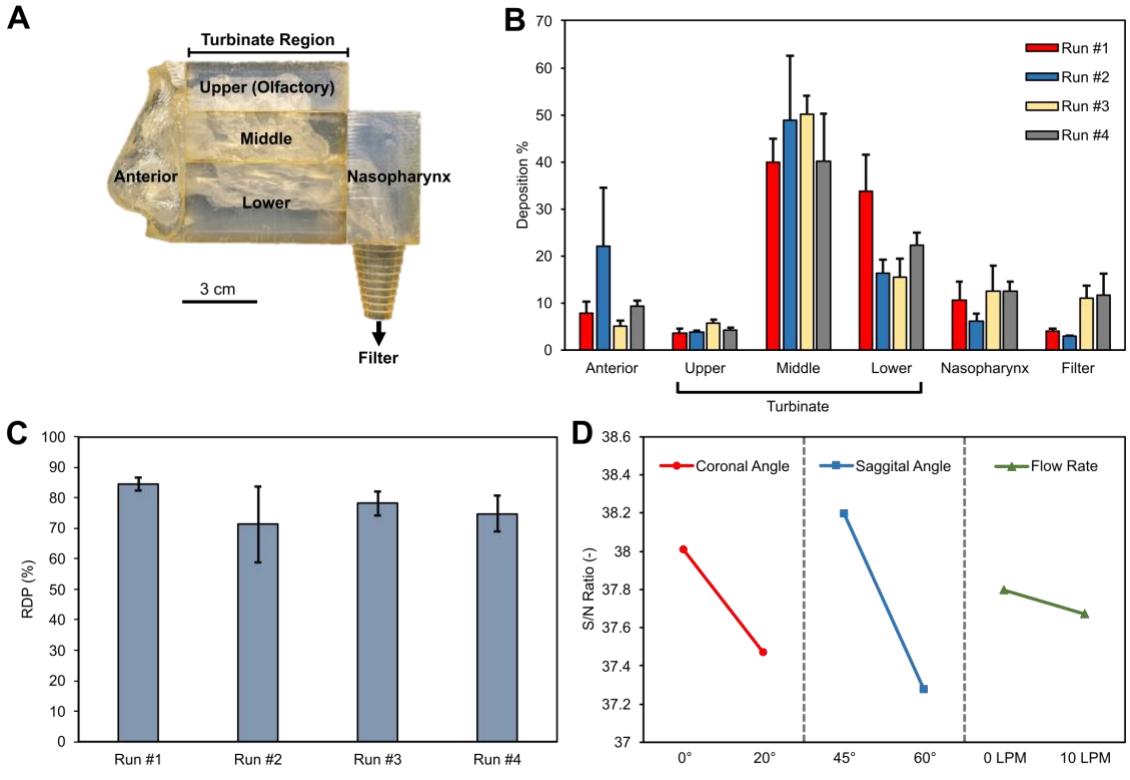

Fig. 11. Deposition patterns of TFF AS01$_B$/OVA/CMC$_{1.9\%}$ vaccine powder in a nasal cast based on a 48-year-old male. (A) A digital image of the nasal cast with different regions labeled. (B) The deposition patterns of the TFF AS01$_B$/OVA/CMC$_{1.9\%}$ powder in different regions. The parameters were designed with the Taguchi array method. (C) The regional deposition efficiency (RDP) of the 4 conditions in the middle and lower turbinate and the nasopharynx regions. (D) The S/N ratio of each parameter at different levels.

The deposition pattern of the TFF AS01$_B$/OVA/CMC$_{1.9\%}$ powder in a nasal cast based on the CT scan of a 7-year-old female is shown in **Fig. 12A-B**. The result showed that most of the TFF AS01$_B$/OVA/CMC$_{1.9\%}$ powder was also deposited in the middle and lower turbinate regions and the nasopharynx region. Compared to the results generated using the adult nasal cast, the differences between different conditions were more significant in the

684 child nasal cast. For example, Run #1 resulted in the highest deposition percentage in the
685 nasopharynx region (**Fig. 12B**), which was desirable for intranasal immunization. This was
686 likely due to the smaller size/depth of the nasal cavity in children, making the effect of
687 these conditions more pronounced. The RDP among 4 conditions ranged from 75.8% to
688 88.8% (**Fig. 12C**), which were generally higher than that of the adult nasal cast. The
689 calculated S/N ratios for all parameters indicated that the optimal condition for the
690 deposition pattern was also: 0° for the coronal angle, 45° for the sagittal angle, and 0 LPM
691 for the flow rate, which is the same as Run #1 (**Fig. 12D**). Different from the adult nasal
692 cast, however, the order of the impact on RDP was: coronal angle > sagittal angle > flow
693 rate.
694
695 Taken together, data in **Fig. 11** and **Fig. 12** showed that in both adult and child nasal casts,
696 the optimal condition to deliver the TFF $AS01_B$/OVA/$CMC_{1.9\%}$ vaccine powder to the
697 middle and lower turbinate and the nasopharynx region was 0° for the coronal angle, 45°
698 for the sagittal angle, and 0 LPM for the flow rate. The insertion depth is expected to also
699 significantly affect the deposition pattern of the TFF vaccine powder sprayed using the
700 UDSP nasal device (Gao et al., 2020). In the present study, for the adult nasal cast, the
701 insertion depth was 0.5 cm and 0.4 cm for the child nasal cast, so that all the parameters in
702 the Taguchi L8 orthogonal array in **Table 1** can be accommodated. Due to the rigid
703 structure of the 3D-printed nasal casts, the insertion depth could not be adjusted in a large
704 interval. Further optimization of the insertion depth may be considered in the future.
705
706 **Fig. sup6A** showed the deposition percentages of the TFF $AS01_B$/OVA/$CMC_{1.9\%}$vaccine
707 powder directly in the nasopharynx region of a 48-year-old male nasal cast in 4 different

runs. The N/S ratios in **Fig. sup6B** indicated that the optimal condition for the TFF vaccine powder to be delivered directly to the nasopharynx region of the nasal cast based on the 48-year-old male is: 0° for the coronal angle, 45° for the sagittal angle, and 10 LPM for the flow rate. The deposition pattern of the TFF $AS01_B$/OVA/$CMC_{1.9\%}$ vaccine powder at the optimal condition identified above is shown in **Fig. sup7**. The percentage of the powder deposited directly in the nasopharynx region was 15.09 ± 4.05%.

Fig. sup8A showed the deposition percentages of the TFF $AS01_B$/OVA/$CMC_{1.9\%}$vaccine powder directly in the nasopharynx region of the 7-year-old female nasal cast in 4 different runs. The N/S ratios in **Fig. sup8B** indicated that the optimal condition for the TFF vaccine powder to be delivered directly to the nasopharynx region of the nasal cast based on the 7-year-old female is 0° for the coronal angle, 45° for the sagittal angle, and 5 LPM for the flow rate. Even at 0° for the coronal angle, 45° for the sagittal angle, and 0 LPM flow rate, the percentage of the powder deposited directly in the nasopharynx region was 35.49 ± 5.14%. Therefore, if one only considers the TFF $AS01_B$/OVA/$CMC_{1.9\%}$ vaccine powder that is directly delivered into the nasopharynx region, where the Waldeyer's ring is located, then applying a flow rate, similar to applying the vaccine to a human subject while the human subject is inhaling, is expected to be beneficial, but there is also an increased chance for the powder to travel beyond the nasopharynx region into the trachea. Direct deposition of a vaccine to the nasopharynx region is important as the vaccine is expected to have a higher chance of reaching the lymphoid tissues (i.e., adenoids and tubal tonsils) in the Waldeyer's ring. If the vaccine is deposited in the posterior nasal cavity, it may ultimately reach the naso-oropharynx region because of the mucous blanket posterior movement, but the lymphoid tissues in the naso-oropharynx need to efficiently interact with the vaccine

732 or antigens bound to the mucus.

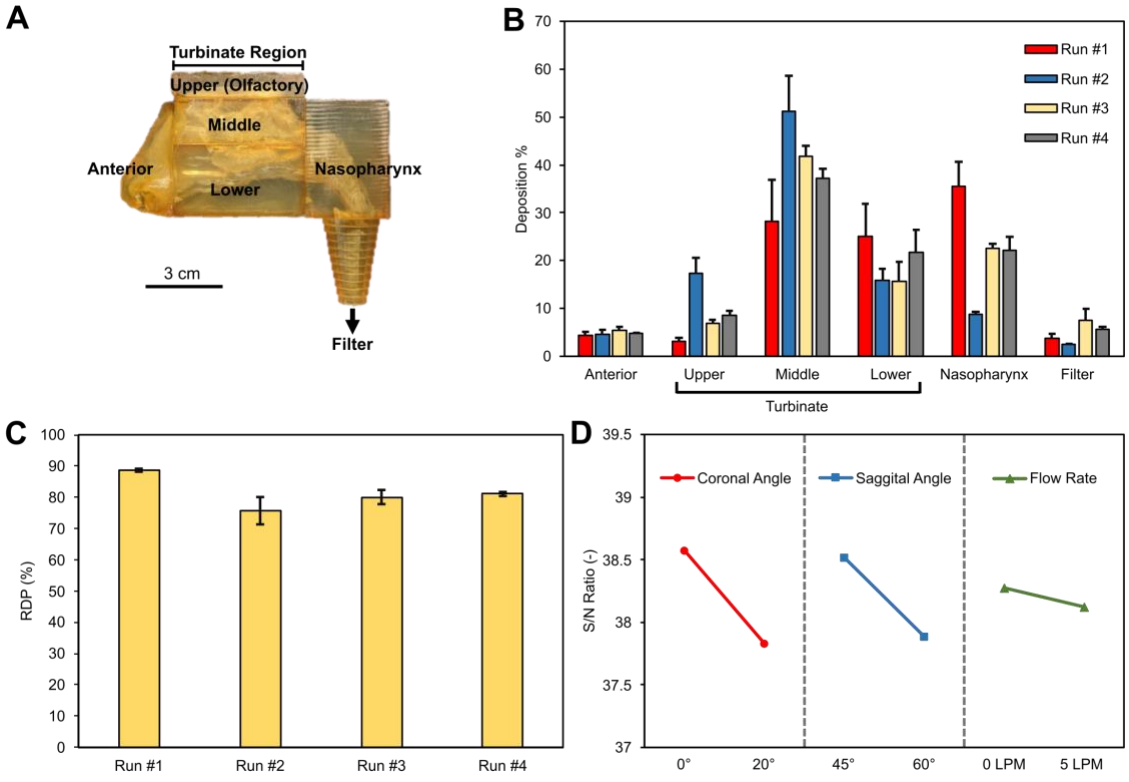

733

734 **Fig. 12.** Deposition pattern of TFF $AS01_B$/OVA/$CMC_{1.9\%}$ vaccine powder in a nasal cast
735 based on a 7-year-old female. (A) A digital image of the nasal cast with different regions
736 labeled. (B) The deposition patterns of the TFF $AS01_B$/OVA/$CMC_{1.9\%}$ powder in different
737 regions. The parameters were designed with the Taguchi array method. (C) The regional
738 deposition efficiency (RDP) of the 4 conditions in the middle and lower turbinate and the
739 nasopharynx regions. (D) The S/N ratio of each parameter at different levels.

740

741 The results reported in this study showed that a protein antigen-based vaccine that is
742 adjuvanted with the liposomal $AS01_B$ adjuvant and contains CMC as a mucoadhesive agent
743 could be converted into a dry powder using the TFF technology and then delivered to the
744 desired regions in nasal casts 3D printed based on the CT-scan images of human noses

using the UDSP nasal device. Besides the AS01$_B$-adjuvanted vaccines, the TFF technology has been successfully applied to various other types of vaccines, including vaccines adjuvanted with aluminum salt (Alzhrani et al., 2021; Li et al., 2015; Thakkar et al., 2018), MF59 or AddaVax (AboulFotouh et al., 2022a), plasmid DNA vaccine (Xu et al., 2022), viral vector-based vaccines (Cui, unpublished data), and messenger RNA-lipid nanoparticle vaccines (Cui, unpublished data). In addition, both Gram-positive and Gram-negative bacteria in suspension can be converted to dry powders using the TFF technology (Wang et al., 2022). Therefore, it is expected that various other types of vaccines can be administered intranasally as TFF powders using the UDSP nasal device to target the vaccines to the lymphoid tissues in the nasopharynx region in humans. Of course, for different vaccines, additional optimization of the formulation and critical processing parameters will likely be needed.

For decades, there has been a strong interest in developing intranasal vaccines. However, as aforementioned, only a few nasal vaccines have received regulatory approval for human use around the world. Many nasal vaccine candidates that are safe and efficacious in preclinical studies often fail to move beyond phase 1 in clinical testing (Cai et al., 2022). For example, the ChAdOx1 nCoV-19 simian adenovirus-based COVID-19 vaccine that was effective in hamsters and non-human primates (NHP) when given intranasally failed to elicit consistent immune responses in humans (Madhavan et al., 2022). The authors hypothesized that the dosage form and the device used to administer the vaccine, both were not optimized for intranasal vaccination, may have contributed, at least in part, to the weak and inconsistent immune responses seen in humans (Madhavan et al., 2022), underscoring the significance of optimizing vaccine formulation and delivery device in nasal vaccine

development.

Nasal vaccines that are currently approved for human use around the world are liquid suspension or freeze-dried powder that must be reconstituted before administration. They are sprayed into the nostrils using a nasal spray system such as the BD Accuspray™. Intranasal immunization using a vaccine dry powder is appealing, but a technology that can transform vaccines from liquid to a dry powder suitable for intranasal delivery, while preserving the physical and chemical properties and immunogenicity of the vaccines is needed. Similarly, a dry powder delivery system that can deliver the vaccine powder to the desired region(s) of the human nasal cavity is also required because there has not been an approved nasal dry powder vaccine for human use yet. Since many intranasal vaccines failed to move beyond phase 1 clinical trials (Cai et al., 2022; Xu et al., 2021b), the formulation of a vaccine intended for intranasal administration must be optimized, and only a device that can efficiently target the vaccine formulation to the desired region(s) in the nasal cavity should be chosen. As aforementioned, in children and adults, the Waldeyer's ring in the naso-oropharynx region is the key lymphoid tissue in the nasal cavity. Therefore, it is ideal to deliver a vaccine powder directly to the nasopharynx region. If the vaccine is delivered in the posterior nasal cavity and binds to the mucus, then it may be carried to the naso-oropharynx region by the mucous blanket posterior movement by means of ciliary clearance, wherein the vaccine may be taken up by the lymphoid tissues in the Waldeyer's ring or cleared through the throat to the stomach and then degraded or deactivated there (Sahin-Yilmaz and Naclerio, 2011). It is possible, or perhaps likely, that some cells in the epithelium of the posterior nasal cavity covered by the mucous layer may be able to take up the vaccine or the antigens, but the vaccine/antigen must penetrate through the mucous

793 layer efficiently and quickly as the mucous blanket posterior movement can clear inhaled
794 particles from the nasal cavity in 10-20 min (Sahin-Yilmaz and Naclerio, 2011).
795
796 A vaccine that is administered/deposited in the region that is anterior to the lower turbinate
797 will be transported anterior out of the nostrils. Testing vaccine powders and delivery
798 devices directly in human subjects is ideal, but less practical. Nasal casts 3D printed based
799 on the CT scan images of the noses of humans of different ages, such as the nasal casts
800 used in the present study and the idealized nasal replica (Chen et al., 2020), provide a
801 suitable alternative for vaccine powder optimization and dry powder delivery device
802 selection. Formulations and devices selected based on nasal casts can then be validated in
803 humans to verify the deposition of the vaccine powder to desired regions or sites before
804 initiating clinical trials to test the safety and efficacy of new vaccine candidates.
805
806
807
808
809
810
811
812
813
814
815
816

4. Conclusion

It is concluded that it is feasible to apply the TFF technology to convert vaccines such as the $AS01_B$-adjuvanted OVA model vaccine with a proper mucoadhesive agent such as CMC into dry powders, and the resultant vaccine powders can be delivered to the desired regions of 3D printed human nasal casts using the UDSP nasal device. The type of the mucoadhesive agents and their concentration were critical so that the physical properties of the vaccine and the integrity of the antigen were preserved after the vaccine was subjected to the TFF technology. The mucoadhesive agent also affected the powder properties of the TFF vaccine powder. When sprayed using the UDSP nasal device, the TFF vaccine powders showed desirable particle size distribution, spray pattern and plum geometry. Importantly, spraying the vaccine powder with the UDSP nasal device did not negatively affect the antigen and the adjuvant. Finally, evaluation of the deposition patterns of TFF $AS01_B$/OVA/$CMC_{1.9\%}$ powder in both adult and child nasal casts showed that the optimal parameters for both nasal casts were: 0° for the coronal angle, 45° for the sagittal angle, and 0 LPM for the flow rate, and more than 80% of the powders were deposited in the middle and lower turbinate and the nasopharynx regions. If only the nasopharynx region is considered, then applying a flow rate was beneficial.

ACKNOWLEDGEMENTS

Z Cui and RO Williams III report financial support from TFF Pharmaceuticals, Inc. The UDSP device was generously provided by the AptarGroup, Inc. Y Yu was supported in part by the Y.L. Lin Hung Tai Education Foundation and the National Taiwan University. K AboulFotouh was supported in part by an Egyptian Government Fellowship. We thank Dr. Hugh Smyth in the College of Pharmacy at UT Austin for letting us use the laser sheet system in his laboratory to acquire the spray pattern and plume geometry data.

DISCLOSURE OF CONFLICT OF INTEREST

Z Cui reports a relationship with TFF Pharmaceuticals, Inc. that includes equity or stocks and research funding. RO Williams III reports a relationship with TFF Pharmaceuticals, Inc. that includes consulting or advisory, equity or stocks, and research funding. Z Cui and RO Williams III report a relationship with Via Therapeutics, LLC that includes equity. Financial conflict of interest management plans are available at UT Austin.

CRediT Author Statement

Y Yu: Conceptualization, Methodology, Investigation, Visualization, Formal analysis, Writing Original Draft; K AboulFotouh: Methodology, investigation; G Williams, J Suman, C Cano: Conceptualization, Resources, Writing-Review & Editing; Z Warnken: Methodology, investigation, Writing-Review & Editing; RO Williams III: Resources, Writing-Review & Editing, Funding acquisition. Z Cui: Conceptualization, Resources, Validation, Writing-Review & Editing, Supervision, Funding acquisition.

5. References

AboulFotouh, K., Uno, N., Xu, H., Moon, C., Sahakijpijarn, S., Christensen, D.J., Davenport, G.J., Cano, C., Ross, T.M., Williams Iii, R.O., Cui, Z., 2022a. Formulation of dry powders of vaccines containing MF59 or AddaVax by Thin-Film Freeze-Drying: Towards a dry powder universal flu vaccine. International Journal of Pharmaceutics 624, 122021.

AboulFotouh, K., Xu, H., Moon, C., Williams, R.O., 3rd, Cui, Z., 2022b. Development of (Inhalable) Dry Powder Formulations of AS01(B)-Containing Vaccines Using Thin-Film Freeze-Drying. Int J Pharm 622, 121825.

Alzhrani, R.F., Xu, H., Moon, C., Suggs, L.J., Williams, R.O., 3rd, Cui, Z., 2021. Thin-Film Freeze-Drying Is a Viable Method to Convert Vaccines Containing Aluminum Salts from Liquid to Dry Powder. Methods Mol Biol 2183, 489-498.

Baldridge, J.R., Yorgensen, Y., Ward, J.R., Ulrich, J.T., 2000. Monophosphoryl lipid A enhances mucosal and systemic immunity to vaccine antigens following intranasal administration. Vaccine 18, 2416-2425.

Beckett, S.T., Francesconi, M.G., Geary, P.M., Mackenzie, G., Maulny, A.P., 2006. DSC study of sucrose melting. Carbohydr Res 341, 2591-2599.

Bhandari, B.R., Hartel, R.W., 2002. Co-crystallization of Sucrose at High Concentration in the Presence of Glucose and Fructose. Journal of Food Science 67, 1797-1802.

Birkhoff, M., Leitz, M., Marx, D., 2009. Advantages of Intranasal Vaccination and Considerations on Device Selection. Indian J Pharm Sci 71, 729-731.

Cai, L., Xu, H., Cui, Z., 2022. Factors Limiting the Translatability of Rodent Model-Based Intranasal Vaccine Research to Humans. AAPS PharmSciTech 23, 191.

Chavda, V.P., Vora, L.K., Pandya, A.K., Patravale, V.B., 2021. Intranasal vaccines for SARS-CoV-2: From challenges to potential in COVID-19 management. Drug Discov Today 26, 2619-2636.

900 Chen, J.Z., Kiaee, M., Martin, A.R., Finlay, W.H., 2020. In vitro assessment of an idealized
901 nose for nasal spray testing: Comparison with regional deposition in realistic nasal replicas.
902 International Journal of Pharmaceutics 582, 119341.
903
904 Davis, S.S., 2001. Nasal vaccines. Advanced Drug Delivery Reviews 51, 21-42.
905
906 Debertin, A.S., Tschernig, T., Tönjes, H., Kleemann, W.J., Tröger, H.D., Pabst, R., 2003.
907 Nasal-associated lymphoid tissue (NALT): frequency and localization in young children.
908 Clin Exp Immunol 134, 503-507.
909
910 Dekina, S., Romanovska, I., Ovsepyan, A., Tkach, V., Muratov, E., 2016.
911 Gelatin/carboxymethyl cellulose mucoadhesive films with lysozyme: Development and
912 characterization. Carbohydr Polym 147, 208-215.
913
914 Engstrom, J.D., Lai, E.S., Ludher, B.S., Chen, B., Milner, T.E., Williams, R.O., 3rd, Kitto,
915 G.B., Johnston, K.P., 2008. Formation of stable submicron protein particles by thin film
916 freezing. Pharm Res 25, 1334-1346.
917
918 Flood, A., Estrada, M., McAdams, D., Ji, Y., Chen, D., 2016. Development of a Freeze-
919 Dried, Heat-Stable Influenza Subunit Vaccine Formulation. PLoS One 11, e0164692.
920
921 Gao, M., Shen, X., Mao, S., 2020. Factors influencing drug deposition in the nasal cavity
922 upon delivery via nasal sprays. Journal of Pharmaceutical Investigation 50, 251-259.
923
924 Gasparini, C., Acunzo, M., Biuso, A., Roncaglia, S., Migliavacca, F., Borriello, C.R.,
925 Bertolini, C., Allen, M.R., Orenti, A., Boracchi, P., Zuccotti, G.V., 2021. Nasal spray live
926 attenuated influenza vaccine: the first experience in Italy in children and adolescents during
927 the 2020-21 season. Ital J Pediatr 47, 225.
928
929 Ghani, J.A., Choudhury, I.A., Hassan, H.H., 2004. Application of Taguchi method in the
930 optimization of end milling parameters. Journal of Materials Processing Technology 145,
931 84-92.
932
933 Grabovac, V., Guggi, D., Bernkop-Schnürch, A., 2005. Comparison of the mucoadhesive
934 properties of various polymers. Adv Drug Deliv Rev 57, 1713-1723.
935

936 Hufnagel, S., Sahakijpijarn, S., Moon, C., Cui, Z., Williams III, R.O., 2022. The
937 development of thin-film freezing and its application to improve delivery of biologics as
938 dry powder aerosols. KONA Powder and Particle Journal, 2022010.
939
940 Kesavan, K., Nath, G., Pandit, J.K., 2010. Sodium alginate based mucoadhesive system for
941 gatifloxacin and its in vitro antibacterial activity. Sci Pharm 78, 941-957.
942
943 Li, X., Thakkar, S.G., Ruwona, T.B., Williams, R.O., Cui, Z., 2015. A method of
944 lyophilizing vaccines containing aluminum salts into a dry powder without causing particle
945 aggregation or decreasing the immunogenicity following reconstitution. Journal of
946 Controlled Release 204, 38-50.
947
948 Lu, Y., Thomas, L.C., Jerrell, J.P., Cadwallader, K.R., Schmidt, S.J., 2017. Investigating
949 the thermal decomposition differences between beet and cane sucrose sources. Journal of
950 Food Measurement and Characterization 11, 1640-1653.
951
952 Madhavan, M., Ritchie, A.J., Aboagye, J., Jenkin, D., Provstgaad-Morys, S., Tarbet, I.,
953 Woods, D., Davies, S., Baker, M., Platt, A., Flaxman, A., Smith, H., Belij-Rammerstorfer,
954 S., Wilkins, D., Kelly, E.J., Villafana, T., Green, J.A., Poulton, I., Lambe, T., Hill, A.V.S.,
955 Ewer, K.J., Douglas, A.D., 2022. Tolerability and immunogenicity of an intranasally-
956 administered adenovirus-vectored COVID-19 vaccine: An open-label partially-
957 randomised ascending dose phase I trial. eBioMedicine, 104298.
958
959 Ortiz, J.R., Goswami, D., Lewis, K.D., Sharmeen, A.T., Ahmed, M., Rahman, M., Rahman,
960 M.Z., Feser, J., Neuzil, K.M., Brooks, W.A., 2015. Safety of Russian-backbone seasonal
961 trivalent, live-attenuated influenza vaccine in a phase II randomized placebo-controlled
962 clinical trial among children in urban Bangladesh. Vaccine 33, 3415-3421.
963
964 Overhoff, K.A., Johnston, K.P., Tam, J., Engstrom, J., Williams, R.O., 2009. Use of thin
965 film freezing to enable drug delivery: a review. Journal of Drug Delivery Science and
966 Technology 19, 89-98.
967
968 Sahin-Yilmaz, A., Naclerio, R.M., 2011. Anatomy and physiology of the upper airway.
969 Proc Am Thorac Soc 8, 31-39.
970
971 Sasaki, S., Hamajima, K., Fukushima, J., Ihata, A., Ishii, N., Gorai, I., Hirahara, F., Mohri,

H., Okuda, K., 1998a. Comparison of intranasal and intramuscular immunization against human immunodeficiency virus type 1 with a DNA-monophosphoryl lipid A adjuvant vaccine. Infection and immunity 66, 823-826.

Sasaki, S., Sumino, K., Hamajima, K., Fukushima, J., Ishii, N., Kawamoto, S., Mohri, H., Kensil, C.R., Okuda, K., 1998b. Induction of systemic and mucosal immune responses to human immunodeficiency virus type 1 by a DNA vaccine formulated with QS-21 saponin adjuvant via intramuscular and intranasal routes. Journal of virology 72, 4931-4939.

Sato-Kaneko, F., Yao, S., Lao, F.S., Sako, Y., Jin, J., Shukla, N.M., Cottam, H.B., Chan, M., Belsuzarri, M.M., Carson, D.A., Hayashi, T., 2022. A Dual Adjuvant System for Intranasal Boosting of Local and Systemic Immunity for Influenza Vaccination. Vaccines 10, 1694.

Sogias, I.A., Williams, A.C., Khutoryanskiy, V.V., 2008. Why is chitosan mucoadhesive? Biomacromolecules 9, 1837-1842.

Suryadevara, M., Domachowske, J.B., 2014. Quadrivalent influenza vaccine in the United States. Hum Vaccin Immunother 10, 596-599.

te Booy, M.P., de Ruiter, R.A., de Meere, A.L., 1992. Evaluation of the physical stability of freeze-dried sucrose-containing formulations by differential scanning calorimetry. Pharm Res 9, 109-114.

Thakkar, S.G., Warnken, Z.N., Alzhrani, R.F., Valdes, S.A., Aldayel, A.M., Xu, H., Williams, R.O., Cui, Z., 2018. Intranasal immunization with aluminum salt-adjuvanted dry powder vaccine. Journal of Controlled Release 292, 111-118.

Trenkel, M., Scherließ, R., 2021. Nasal Powder Formulations: In-Vitro Characterisation of the Impact of Powders on Nasal Residence Time and Sensory Effects. Pharmaceutics 13, 385.

Wang, J.-L., Kuang, M., Xu, H., Williams, R.O., Cui, Z., 2022. Accelerated mass transfer from frozen thin films during thin-film freeze-drying. bioRxiv, 2022.2004.2016.488553.

Wang, J.L., Hanafy, M.S., Xu, H., Leal, J., Zhai, Y., Ghosh, D., Williams Iii, R.O., David

1008 Charles Smyth, H., Cui, Z., 2021. Aerosolizable siRNA-encapsulated solid lipid
1009 nanoparticles prepared by thin-film freeze-drying for potential pulmonary delivery. Int J
1010 Pharm 596, 120215.
1011
1012 Warnken, Z.N., Smyth, H.D.C., Davis, D.A., Weitman, S., Kuhn, J.G., Williams, R.O.,
1013 2018. Personalized Medicine in Nasal Delivery: The Use of Patient-Specific
1014 Administration Parameters To Improve Nasal Drug Targeting Using 3D-Printed Nasal
1015 Replica Casts. Molecular Pharmaceutics 15, 1392-1402.
1016
1017 Xu, H., Bhowmik, T., Gong, K., Huynh, T.N.A., Williams, R.O., Cui, Z., 2021a. Thin-film
1018 freeze-drying of a bivalent Norovirus vaccine while maintaining the potency of both
1019 antigens. International Journal of Pharmaceutics 609, 121126.
1020
1021 Xu, H., Cai, L., Hufnagel, S., Cui, Z., 2021b. Intranasal vaccine: Factors to consider in
1022 research and development. International Journal of Pharmaceutics 609, 121180.
1023
1024 Xu, H., Moon, C., Sahakijpijarn, S., Dao, H.M., Alzhrani, R.F., Wang, J.-l., Williams, R.O.,
1025 Cui, Z., 2022. Aerosolizable plasmid DNA dry powders engineered by thin-film freezing.
1026 bioRxiv, 2022.2010.2003.510625.
1027
1028 Zhang, Y., Soto, M., Ghosh, D., Williams, R.O., 2021. Manufacturing Stable Bacteriophage
1029 Powders by Including Buffer System in Formulations and Using Thin Film Freeze-drying
1030 Technology. Pharmaceutical Research 38, 1793-1804.
1031

Supplementary Material

S1. Preparation of the OVA-FITC. OVA and (240 mg) and FITC (12 mg) were dissolved in 60 mL of 0.1 M sodium carbonate/bicarbonate solution (pH = 9). The mixture was stirred overnight at room temperature. After the reaction, the buffer and the unreacted FITC were removed by centrifugation with 30,000 MWCO centrifugal filter tubes from Millipore (Grand Island, NY, USA). The FITC-OVA was then washed 4 times with 20 mL of PBS. To purify the FITC-OVA, the mixture was further centrifuged with the 100,000 MWCO centrifugal filter tubes, and the filtrate (i.e., OVA-FITC in PBS) was collected.

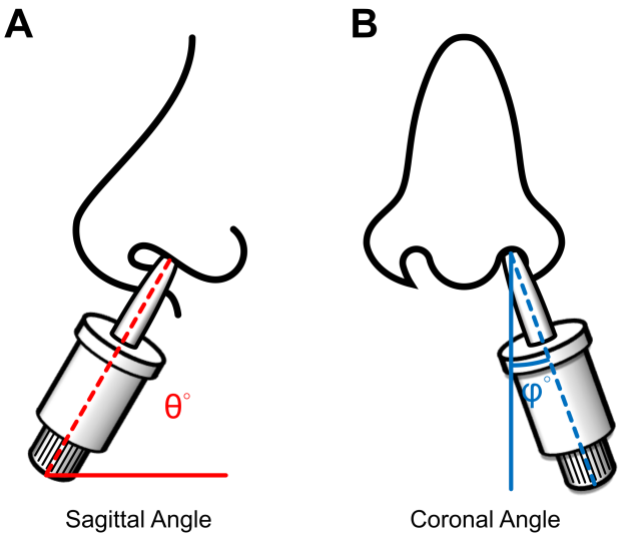

Fig. sup1. The definition of the coronal angle and the sagittal angle.

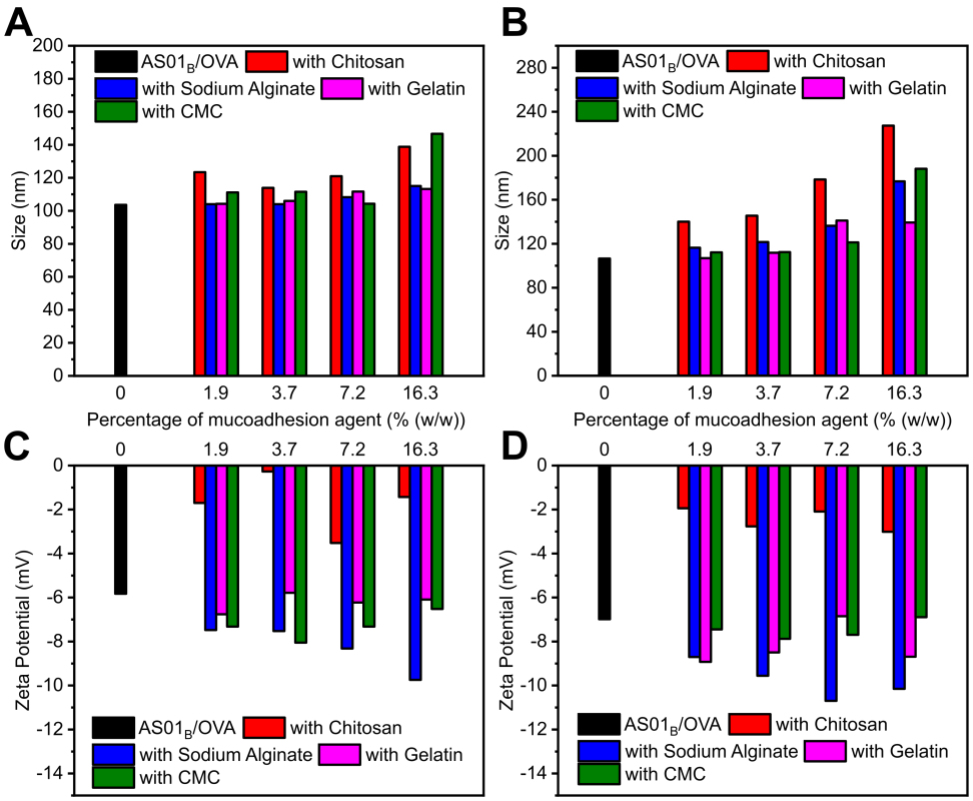

Fig. sup2. Particle size and zeta potential of AS01$_B$/OVA without or with different concentrations of mucoadhesive agents before (A, C) and after being subjected to thin-film freeze-drying (B, D) (n = 1).

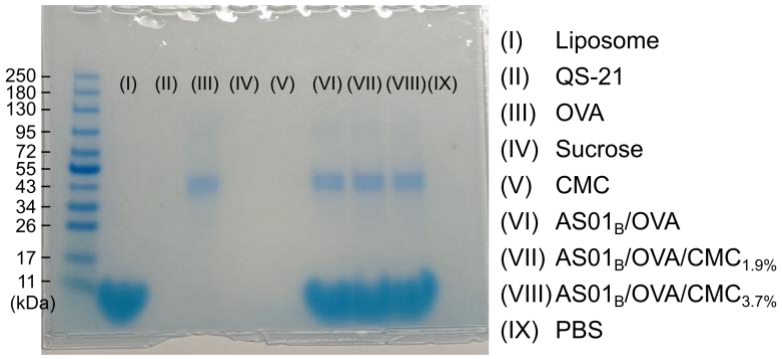

Fig. sup3. SDS-PAGE images of the $AS01_B$/OVA vaccine with 0, 1.9, and 3.7% of CMC and their individual component (i.e., liposome, QS21, OVA, sucrose, CMC, PBS).

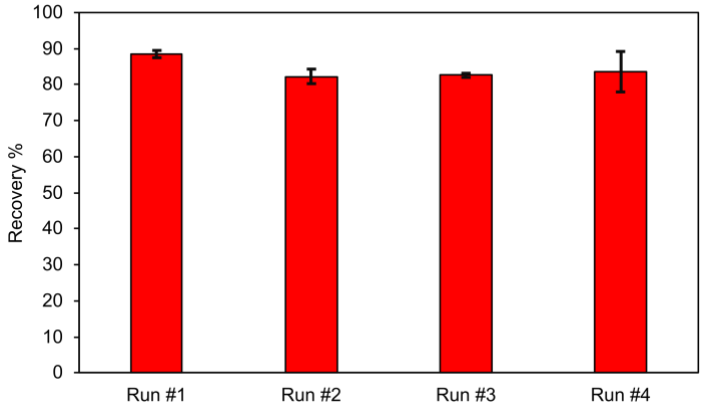

Fig. sup4. The recovery percentage of the TFF $AS01_B$/OVA/$CMC_{1.9\%}$ vaccine powder in the 48-year-old male nasal cast.

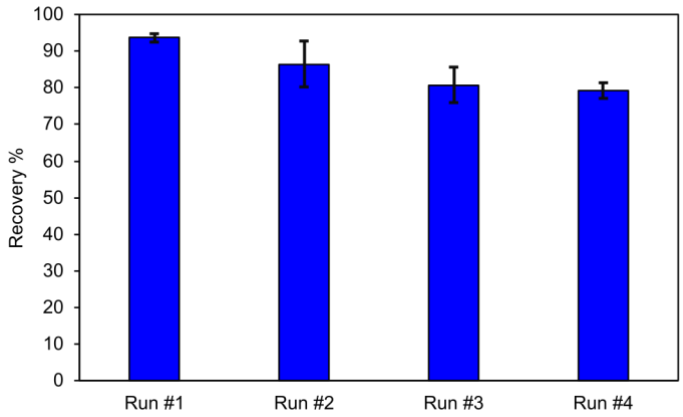

Fig. sup5. The recovery percentage of the TFF AS01$_B$/OVA/CMC$_{1.9\%}$ vaccine powder in the 7-year-old female nasal cast.

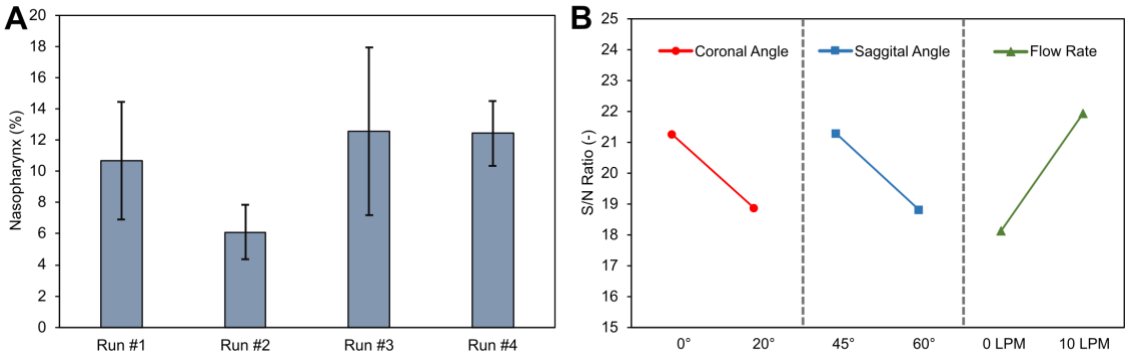

Fig. sup6. (A) The deposition percentage of the TFF $AS01_B$/OVA/$CMC_{1.9\%}$vaccine powder in the nasopharynx region of a 48-year-old male nasal cast. (**B**) The S/N ratio of each parameter at different levels.

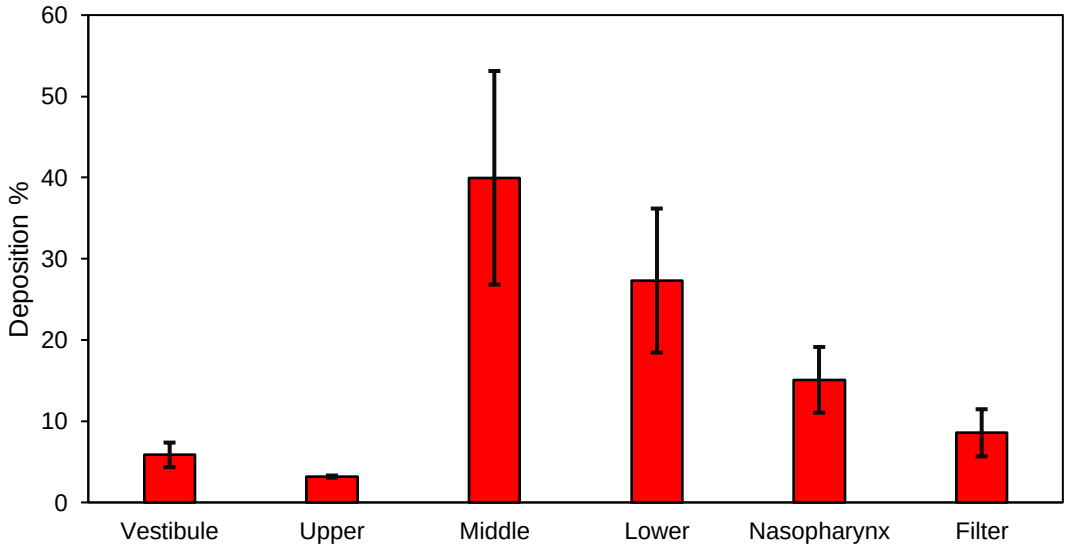

Fig. sup7. The deposition percentage of the TFF $AS01_B$/OVA/$CMC_{1.9\%}$ vaccine powder in the nasopharynx region of a 48-year-old male nasal cast when applied using a UDSP nasal device at the following condition: coronal angle = 0°, sagittal angle = 45°, flow rate = 10 LPM.

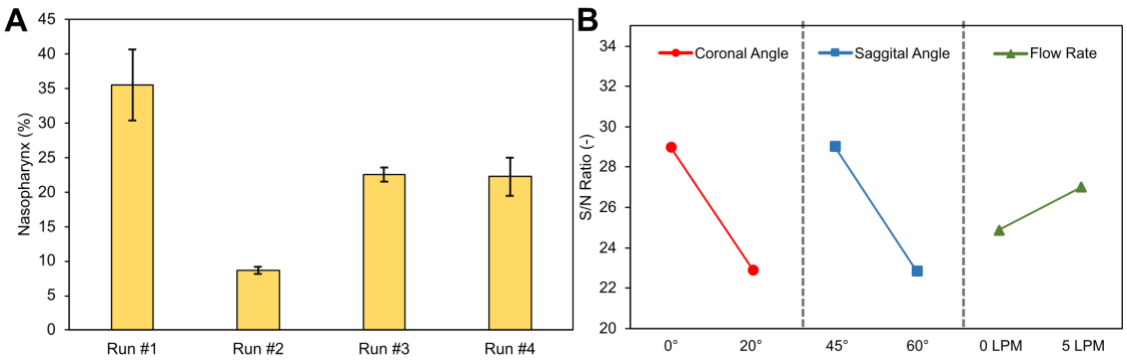

Fig. sup8. (**A**) The deposition percentage of the TFF $AS01_B$/OVA/$CMC_{1.9\%}$ vaccine powder in the nasopharynx region of a 7-year-old female nasal cast. (**B**) The S/N ratio of each parameter at different levels.